

Analyzing Fine-tuning Representation Shift for Multimodal LLMs Steering

Pegah Khayatan^{*1} Mustafa Shukor^{*1} Jayneel Parekh^{*1} Matthieu Cord^{1,2}

¹ISIR, Sorbonne Université, Paris, France ²Valeo.ai, Paris, France

Abstract

Multimodal LLMs have reached remarkable levels of proficiency in understanding multimodal inputs, driving extensive research to develop increasingly powerful models. However, much less attention has been paid to understanding and explaining the underlying mechanisms of these models. Most existing explainability research examines these models only in their final states, overlooking the dynamic representational shifts that occur during training. In this work, we systematically analyze the evolution of hidden state representations to reveal how fine-tuning alters the internal structure of a model to specialize in new multimodal tasks. Using a concept-based approach, we map hidden states to interpretable visual and textual concepts, enabling us to trace changes in encoded concepts across modalities as training progresses. We also demonstrate the use of shift vectors to capture these concepts changes. These shift vectors allow us to recover fine-tuned concepts by shifting those in the original model. Finally, we explore the practical impact of our findings on model steering, showing that we can adjust multimodal LLMs behaviors without any training, such as modifying answer types, captions style, or biasing the model toward specific responses. Our work sheds light on how multimodal representations evolve through fine-tuning and offers a new perspective for interpreting model adaptation in multimodal tasks. The code for this project is publicly available at <https://github.com/mshukor/xl-vllms>.

1. Introduction

With the rapid progress in Large Language Models (LLMs) [7, 10, 22, 34, 52], Multimodal LLMs (MLLMs) [3, 11, 27, 30] have recently demonstrated remarkable capabilities in addressing complex multimodal tasks such as image captioning and visual question-answering.

MLLMs are typically composed of a visual encoder, an LLM, and an intermediary connector. Following initial unimodal pretraining—and, in many cases, multimodal pretraining on large datasets—these models can be further spe-



Figure 1. **Overview.** We analyse the concepts representations change due to fine-tuning. This has direct implications on steering MLLMs without any extra training.

cialized by training on multimodal datasets [1, 26]. Given the high computational cost of training these models, recent research has proposed more efficient approaches, such as creating diverse, high-quality instruction-tuning datasets [30] or keeping the LLM frozen and fine-tuning small amount of model parameters, like the connector [31, 46, 47, 54]. These approaches take advantage of the impressive ability of frozen LLMs to generalize to multimodal data [45]. Despite the different efficient tuning methods, training these models still incurs significant cost due to backpropagating the gradient through large models.

While substantial progress has been made in developing high-performing MLLMs, relatively few studies aim to understand them [4, 37, 44, 45, 48, 60]. Existing work typically conducts post-hoc analyses of MLLMs in isolation, overlooking the internal changes during fine-tuning. Research by [45] addresses this gap to some extent by examining the internal multimodal alignment as it evolves during training.

In contrast, we focus on exploring how MLLMs update their internal semantic representations when fine-tuned for multimodal tasks (see Fig. 1). Understanding how fine-tuning alters learned concepts—and, consequently, the features encoded by the model—opens the possibility of directly modifying these features to steer model outputs, reducing the need for additional training and its associated costs.

Our approach leverages concept-based explainability to investigate how concept representations evolve from the orig-

inal model to its fine-tuned version. We find that fine-tuning on a specific task reshapes these concepts, with some adjusting subtly to align with the task, and others emerging or disappearing altogether (see Fig. 2). Notably, most fine-tuned concepts can be reconstructed from the original model by translating its original concepts along specific shift vectors. Lastly, we explore the implications of this study for steering MLLMs, demonstrating how model responses can be modified without additional training. Our key findings are summarized as follows:

- We show that learned concepts adapt specifically to the fine-tuning task, with some concepts becoming more specialized and others undergoing complete transformation.
- Many of the concepts encoded in the fine-tuned model can be reconstructed from those in the original model using shift vectors in the latent space.
- We apply these findings to steer MLLMs (e.g., LLaVA) outputs, demonstrating the possibility to steer the model’s answers or response style. To the best of our knowledge, this is the first work exploring MLLMs steering.

2. Related Work

Concept-based explainability. Concept-based explainability methods have emerged as an alternative to traditional feature attribution based methods, that are capable of extracting key semantic features from the model internal representations. Most post-hoc concept explainability approaches are based on the idea of concept activation vectors (CAV) [23], which represent concepts as vectors in the activation space. Instead of relying on human annotations, recent works have proposed methods to automatically discover concepts via clustering [17, 57] or matrix decomposition [14], which can be viewed as instances of a dictionary learning problem [13]. Initially focusing on understanding vision models, dictionary learning for concept extraction has been extended to LLMs, for instance, in the form of sparse autoencoders [21, 41]. However, none of the prior approaches have been applied to understand multimodal models, with the exception of recently proposed CoX-LMM [37].

MLLMs and Explainability. Multimodal LLMs [3, 27, 30, 54] have recently garnered significant interest. These models generally adopt a late fusion architecture, which includes an image encoder [15, 40, 58], a connector module, and an LLM [22, 50, 52]. This family of models has inspired extensive research to better understand them and explain their behavior. For example, studies like [20, 35, 44] seek to identify multimodal neurons within LLMs or analyze modality-specific sub networks [45]. Given that these models are text-generative, some methods leverage this property to simply generate textual explanations for model outputs [9, 16, 48, 56]. Based on LLMs, multimodal models benefit from in-context learning capabilities, which have been examined for limitations, including biases [4] and links to

hallucinations [48], as well as the factors that may enhance their in-context learning performance [8, 39]. Related to our approach, CoX-LMMs [37] employs dictionary learning to extract multimodal semantic concepts from model representations. However, these studies typically assess models only in their final trained states, overlooking the dynamic changes that occur during training. Only limited works, such as [45], have investigated this training process, focusing specifically on implicit alignment between image and text modalities. In this work, we investigate how multimodal concepts within the model evolve throughout fine-tuning and explore the implications of these shifts on model steering.

Steering models with feature editing. In contrast to editing model weights, representation or feature editing methods [49, 53, 55] aim to modify model outputs without altering the model’s weights. A prominent approach within this family involves identifying steering vectors, or directions in the feature space (often within the residual stream), that are linked to contrasting concepts. These methods have been applied to language models for various purposes, such as enhancing factuality or reducing hallucinations [36], inducing sentiment shifts or detoxification [51, 53], improving refusals to harmful requests [2], promoting truthfulness by modifying the output of attention heads [28], and erasing specific concepts or biases [6, 42]. However, these techniques have primarily focused on language models, with their application to MLLMs yet to be explored.

3. Notations and Background

This section covers the background and the notations.

Model architecture. A generic MLLM consists of a visual encoder f_V , a trainable connector C , and a language model f_{LM} . We assume that the model is pretrained on a multimodal dataset $\mathcal{S} = \{(x_i, y_i)\}_i$, such as captioning, where $x_i \in \mathcal{X}$ represents images and $y_i \subset \mathcal{Y}$ are the associated captions specified as sequence of tokens from token vocabulary space \mathcal{Y} . The model is trained to generate the next text tokens, conditioned on text and images. The input to f_{LM} is a sequence of tokens that includes the concatenation of: (1) N_V visual tokens extracted from the image x via the visual encoder followed by the connector ($C(f_V(x))$), and (2) linearly embedded textual tokens corresponding to the text instruction and previously predicted tokens. This can be expressed as:

$$\hat{y}^p = f_{LM}(h^1, \dots, h^{N_V}, \dots, h^p),$$

where $h^1, \dots, h^{N_V} = C(f_V(x))$, and $h^p = \text{Emb}(\hat{y}^{p-1})$, with Emb representing the token embedding layer. During generation, the output token \hat{y}^p is derived by normalizing the last layer (L) tokens $h_{(L)}^p$, then applying the unembedding layer W_U and a softmax operation. The model keeps

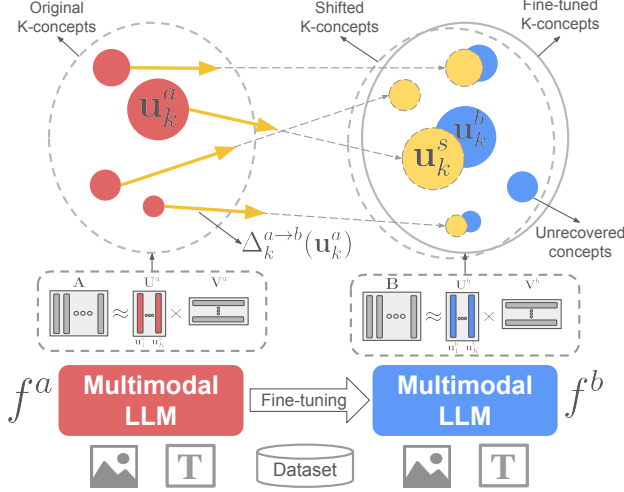


Figure 2. **Analysis framework overview.** We analyse the concepts representation change during fine-tuning and derive shift vectors that can recover most of the concept in the fine-tuned model.

predicting the next token until the end of the sentence token to obtain the generated response $\hat{y} = \{\hat{y}^p\}_{p > N_V + N_I}$, where N_I corresponds to the text instruction.

Concept-based explainability. To understand the internal representations of any given MLLM f , we leverage the approach introduced in [37]. Specifically, for a token of interest TOI , we first extract the residual stream representations, after the l -th layer, $h_{(l)}^p = f_l(x)$ [12] of a subset of samples $X_{TOI} \subset \mathcal{S}$. X_{TOI} includes all the samples x that contain TOI in both the ground truth and predicted response ($TOI \in \hat{y}; \hat{y} = f(x)$). For simplicity, given a sample x_m the extracted hidden states (or features) corresponding to the TOI token is denoted as $z_m = f_l(x_m) \in \mathbb{R}^D$, where D is the features dimension. Thus the features from all samples gives a feature matrix $Z \in \mathbb{R}^{D \times M}$ where $M = |X_{TOI}|$. The feature matrix Z is then decomposed as $Z \approx UV$ to discover the encoded concepts. Here, $U \in \mathbb{R}^{D \times K}$ is the matrix of K concepts and $V \in \mathbb{R}^{K \times M}$ represents the coefficients/activations of the samples projected onto these concepts. Each column $u_k \in U$ corresponds to a concept, while each column of V encodes the activation of these concepts for a given sample. Note that any given representation $f_l(x)$ can be projected on U to obtain its activation vector $v(x) \in \mathbb{R}^K$, i.e. $f_l(x) \approx Uv(x)$.

Each extracted concept is interpreted through grounding in both image and text spaces. Specifically, the top N_{MAS} most activating samples for the concept u_k represent its image grounding X_{MAS}^a :

$$X_{MAS}^a(u_k) = \arg \max_{\hat{X} \subset \mathbf{X}_t, |\hat{X}|=N_{MAS}} \sum_{x \in \hat{X}} |v_k(x)|, \quad (1)$$

where $v_k(x)$ refers to the the activation of u_k for image

x . For text grounding, we decode the features using the unembedding matrix of the language model W_U [5, 25, 33, 43]. Specifically, the operation $W_U u_k \in \mathbb{R}^{|\mathcal{V}|}$ produces logits over the vocabulary, and the top $N_{grounding}$ words with highest logits are extracted:

$$T_{words}^a(u_k) = \arg \max_{\text{Top-}N_{grounding}} (W_U u_k). \quad (2)$$

We employ K -Means to learn our concept dictionaries. This is motivated by K -Means' simplicity, and straightforward arithmetic manipulation of the clusters/concepts it allows, making it a more suitable for our analysis.

Fine-tuning setup. To develop a specialized model f^b tailored for a particular task—or, specifically, for a set of target concepts—the original model f^a is fine-tuned on samples that include a set of words, $\{w_1, \dots, w_m\}$, associated with these target concepts. Our focus is on fine-tuning the LLM component, using Low-Rank Adaptation (LoRA) [19], an approach known to deliver performance comparable to full model fine-tuning while being significantly more efficient [27, 30]. After finetuning, we extract feature matrices $A \in \mathbb{R}^{D \times M^a}$ ($M^a = |X_{TOI}^a|$) from f^a and $B \in \mathbb{R}^{D \times M^b}$ ($M^b = |X_{TOI}^b|$) from f^b , which contain the set of residual stream representations composed of:

$$a_i = f_l^a(x_i^a), \quad b_j = f_l^b(x_j^b),$$

where $x_i^a \in X_{TOI}^a$ and $x_j^b \in X_{TOI}^b$ are samples where TOI is present in the ground truth and the response of both f^a and f^b . Next, the matrices A and B are decomposed to extract the concepts each encodes as:

$$A \approx U^a V^a, \quad B \approx U^b V^b,$$

where the hidden states of each sample can be represented as $a_i = U^a v^a(x_i^a)$ and $b_j = U^b v^b(x_j^b)$, U^a with $U^b \in \mathbb{R}^{D \times K}$ representing the learned concepts $\{u_k^a\}_{k=1}^K, \{u_k^b\}_{k=1}^K$ respectively, and V^a and $V^b \in \mathbb{R}^{K \times M}$ are the corresponding activations. Finally, we ground the concepts in the image modality (Eq. (1)) to obtain $X_{k,MAS}^a$ and $X_{k,MAS}^b$ as well as in the text modality (Eq. (2)) to obtain T_{words}^a and T_{words}^b .

Concepts similarity. To quantify the similarity of two concepts u and u' , we define *Text Grounding Overlap* between them as:

$$T\text{-Overlap}(u, u') = 100 \times \frac{|T_{words}^a(u) \cap T_{words}^a(u')|}{|T_{words}^a(u)|}. \quad (3)$$

One can similarly define the *Image Grounding Overlap* and discussed in the Appendix.



Figure 3. **Concepts extracted from original and fine-tuned models.** Illustration of concepts groundings, for $TOI = \text{person}$, extracted from f^a (top), and f^b which is fine-tuned to focus more on places. Notably, the concepts from f^b exhibit a stronger association with places.

4. Fine-tuning and evolution of concept representations

We aim to study how fine-tuning process affects the concepts learned by the model. Then we try to recover the fine-tuned model concepts using shift vectors computed in the feature space.

Implementation details. We focus on MLLMs with the architecture described in Section 3. The image encoder f_V is a ViT-L/14 CLIP [40], followed by a transformer-based connector that reduce the number of encoded visual tokens. The LLM f_{LM} is an OPT-6.7B model [59] with 32 layers. We conduct our study in a controlled setups that consists of specializing the model on a target dataset. Specifically, we fine-tune on three different subsets of the Visual Genome dataset [24], related to places, colors, and sentiments (see App. A for more details).

4.1. Impact of fine-tuning on learned concepts

The fine-tuning process introduces changes in the overall structure of the learned concepts. This change can be observed through the concepts groundings in both the text and image space (Fig. 3).

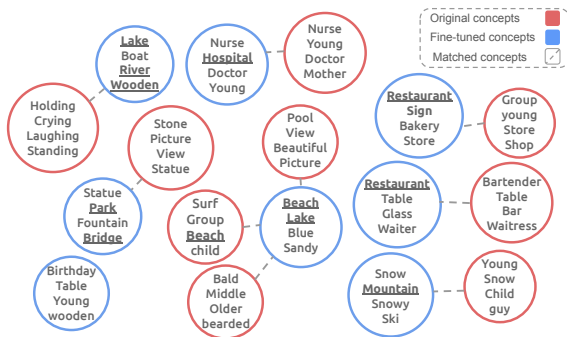


Figure 4. **Concepts text grounding change after fine-tuning.** Illustration of text grounding for concepts ($TOI = \text{person}$) from f^a and their match from f^b , after fine-tuning to focus more on places.

Matched concepts. To analyze how each concept changes after fine-tuning, we focus on each concept and its match

(see Fig. 4). Specifically, we define a matching function $m : i \rightarrow j^*$ which associates each concept vector \mathbf{u}_i^a in set U^a to its closest vector $\mathbf{u}_{j^*}^b$ in set U^b based on cosine similarity, i.e:

$$m(i) = \arg \max_{\mathbf{u}_{j^*}^b \in U^b} \cos(\mathbf{u}_i^a, \mathbf{u}_{j^*}^b), \quad \cos(\mathbf{u}_i^a, \mathbf{u}_{j^*}^b) = \frac{\mathbf{u}_i^a \cdot \mathbf{u}_{j^*}^b}{\|\mathbf{u}_i^a\| \|\mathbf{u}_{j^*}^b\|} \quad (4)$$

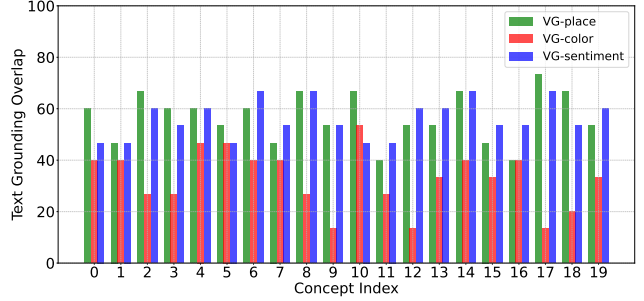


Figure 5. **Text grounding overlap between original and fine-tuned models.** Illustration of T-Overlap between original and matched fine-tuned model concepts.

Concept evolution. To quantify how much a concept $\mathbf{u}_i^a \in U^a$ is changed after fine-tuning, we compute the overlap between its grounding words and those of its closest matching concept from the fine-tuned model U^b . Specifically, we compute $T\text{-Overlap}(\mathbf{u}_i^a, \mathbf{u}_{m(i)}^b)$ (Eq. (3)) for all the concepts $i \in \{1, \dots, K\}$, and visualize them for different fine-tunings in Fig. 5. We observe varying rates of change across different concepts and fine-tunings. This might be due to the difference in the fine-tuning dataset size, complexity, or similarity to the original dataset. It also highlights 2 main behaviors, detailed as follows:

- *Concepts that are refined.* This group contains the concepts that slightly change to be more specialized towards the fine-tuning task (Fig. 6a). These concepts exhibit a relatively high ($T\text{-Overlap}(\mathbf{u}_i^a, \mathbf{u}_{m(i)}^b)$).
- *Concepts that change completely.* This group contains the concepts that emerge (Fig. 6b) or disappear (Fig. 6c) in the fine-tuned model. New concepts emerge in the fine-tuned model, likely due to the introduction of novel patterns or relationships not present in the original model. These concepts exhibit a relatively low ($T\text{-Overlap}(\mathbf{u}_i^a, \mathbf{u}_{m(i)}^b)$).

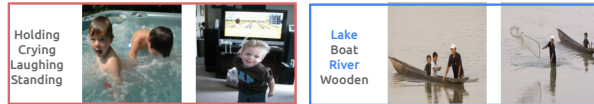
We also notice that the T-Overlap decreases with the number of training iterations, indicating that fine-tuning leads to deviation from original model concepts (see App. A for more details).



(a) **Refined concepts:** fine-tuned model concepts show more grounding to places.



(b) **Emerg concepts:** only fine-tuned model concepts show groundings related to places.



(c) **Diminished concepts:** original model concepts (actions) disappeared after fine-tuning.

Figure 6. **Concepts evolve differently due to fine-tuning.** Left: concepts extracted from the original model f^a . Right: concept extracted from f^b , fine-tuned to focus on places. Each concept is grounded in image and text.

4.2. Recovering concepts in fine-tuned model via shift vectors

In this section, we study if the learned concepts in the fine-tuned model can be recovered from the original model concepts, without any training or decomposition. In particular, we propose to characterize the change in original concepts due to fine-tuning as linear directions in the feature space, referred to these as *concept shift vectors*.

Shifting original model concepts. To compute the concept shift vectors, we first associate each concept \mathbf{u}_k^a in the original model with a subset of samples common to the analysis of both f^a and f^b . Specifically, projecting the representation of each sample $x_m \in \mathbf{X}_{TOI}^a \cap \mathbf{X}_{TOI}^b$ on \mathbf{U}^a and selecting those that activate \mathbf{u}_k^a the most:

$$\mathbf{A}_k = \{m \mid k = \arg \max_i |\mathbf{v}_i^a(x_m)|\}.$$

For each sample $x_m, m \in \mathbf{A}_k$ we define $\delta_m^{a \rightarrow b} = \mathbf{b}_m - \mathbf{a}_m$ as the change in its representation from f^a to f^b . To compute the concept shift vector $\Delta_k^{a \rightarrow b}(\mathbf{u}_k^a)$ associated with \mathbf{u}_k^a , we aggregate shifts of its associated samples specified by \mathbf{A}_k :

$$\Delta_k^{a \rightarrow b}(\mathbf{u}_k^a) = \frac{1}{|\mathbf{A}_k|} \sum_{m \in \mathbf{A}_k} \delta_m^{a \rightarrow b} = \frac{1}{|\mathbf{A}_k|} \sum_{m \in \mathbf{A}_k} (\mathbf{b}_m - \mathbf{a}_m)$$

The concept shift vector is used to shift each concept in the original model \mathbf{u}_k^a to obtain the shifted concept \mathbf{u}_k^s :

$$\mathbf{u}_k^s = \mathbf{u}_k^a + \alpha \Delta_k^{a \rightarrow b}(\mathbf{u}_k^a), \quad (5)$$

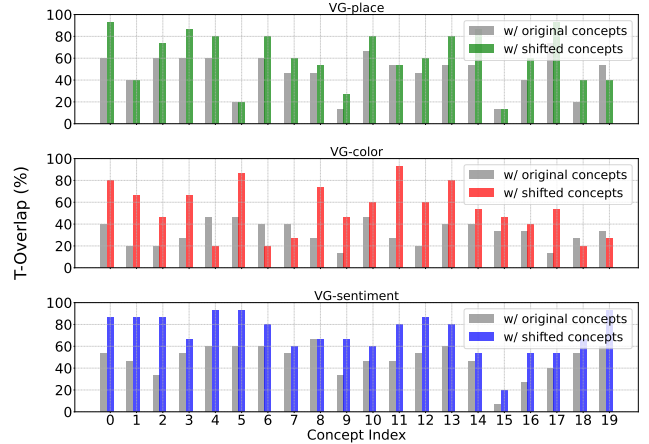


Figure 7. **Recovering fine-tuned model concepts.** For each matched fine-tuned concept we report its text grounding overlap with the original concept and the shifted concept. Model fine-tuned on: places (top), colors (middle) and sentiments (bottom).

where α is a coefficient to control the shift magnitude. Unless otherwise stated, we use $\alpha = 1$ as the default magnitude of shift. It is worth noting that given the concept shift vectors, the computation of shifted concepts does not rely on accessing the fine-tuned model.

Evaluating fine-tuned concept recovery. To study if the fine-tuned concepts \mathbf{U}^b can be recovered from the original ones \mathbf{U}^a , we first establish a matching ($m : i \rightarrow j$) between the set of original $\{\mathbf{u}_i^a\}_{i=1}^K$ and fine-tuned concepts $\{\mathbf{u}_j^b\}_{j=1}^K$. For systematic evaluation of recovery of all fine-tuned concepts, we constrain m to be bijective (see App. A for more details). Finally, we evaluate how well a shifted concept \mathbf{u}_k^s is similar to its match $\mathbf{u}_{m(k)}^b$ using the overlap metrics. Fig. 7 shows the results of recovering the fine-tuned concepts for models fine-tuned on different subsets of the VG dataset (place, color, sentiment). We compare the text grounding overlap between the shifted \mathbf{u}_k^s and fine-tuned concepts $\mathbf{u}_{m(k)}^b$. We use the overlap between the original concepts \mathbf{u}_k^a with the fine-tuned ones as a baseline. As we can see, most shifted concepts exhibit higher overlap than the original ones. Many of them have very high overlap close to 100% (full recovery).

Shift magnitude (α) and concepts recovery. We also study the amount of recovery for shifted concepts, obtained with different shift magnitudes α . We report the average recovery over $K = 20$ concepts for each fine-tuning task for different α values in Fig. 8. Note that $\alpha = 0$ corresponds to original concepts. $\alpha = 1$ generally corresponds to the most optimal value of shift magnitude (color, sentiment fine-tuning) or very close to the optimal value (place fine-tuning). This indicates that simply adding the mean shift vector to the original concept without scaling, generally offers the best

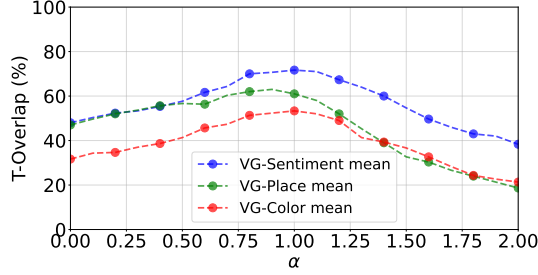


Figure 8. **Shift magnitude (α) and recovering fine-tuned model concepts.** Illustration of the average of T-Overlap between shifted and matched fine-tuned concepts when varying the shift magnitude.

possibility to recover the fine-tuned concepts.

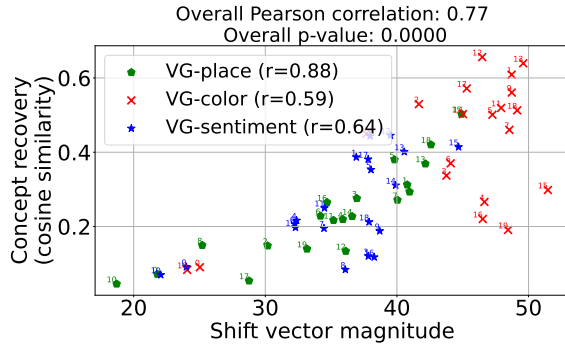


Figure 9. **Correlation between shift vector magnitudes and concept recovery.** Each point corresponds to an original concept from models fine-tuned on 3 VG subsets. The higher the shift vector magnitude the better the concept recovery.

Which concepts are recovered? We examine the potential correlation between the computed concept shift vectors and the recovery of concepts in the fine-tuned model. We hypothesize that if samples related to an original concept consistently and significantly shift toward the corresponding fine-tuned model concepts, the shift vector, computed based on these samples, should be more effective at recovering this concept. Assuming that individual shifts $\delta_m^{a \rightarrow b}$ associated with each original concept tend to have similar magnitudes, their aggregation $\Delta_k^{a \rightarrow b}$ should have a higher magnitude when they are aligned. We validate that this assumption is reasonable for most concepts in our analysis (App. A).

For discovered concepts across all three fine-tuning tasks, we measure the correlation between the magnitude of the concept shift vectors $\|\Delta_k^{a \rightarrow b}\|$ and concepts recovery, here, measured as the cosine similarity between the shifted and matched fine-tuned concept. For a given shifted concept \mathbf{u}_k^s ,

this recovery (CR) is calculated as:

$$CR_k = \frac{\cos(\mathbf{u}_{m(k)}^b, \mathbf{u}_k^s) - \cos(\mathbf{u}_{m(k)}^b, \mathbf{u}_k^a)}{\cos(\mathbf{u}_{m(k)}^b, \mathbf{u}_k^a)} \quad (6)$$

This is illustrated in Fig. 9, where we observe a noticeable correlation between the two quantities, which further strengthens our hypothesis.

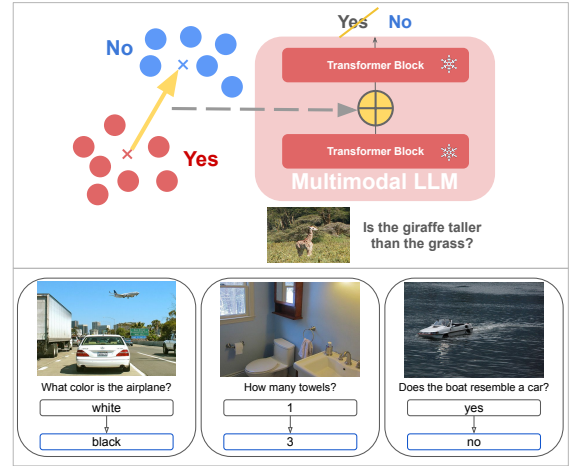


Figure 10. **Steering MLLMs answers.** **Top:** overview of the steering framework. We add a steering vector to the residual stream of MLLMs to change its response. **Bottom:** Each example corresponds to different steering vector that change a specific original answer (e.g., white) to a target one (e.g., black).

5. Fine-grained multimodal LLM steering

Model steering (see Fig. 10) refers to guiding the model outputs towards desired outcomes by modifying the features without altering the model weights. Here, we investigate this technique, focusing on large multimodal models for visual question-answering and image captioning tasks. We provide additional qualitative results and ablation study in App. B.

Motivation. In the previous sections, we demonstrate the feasibility of recovering target concepts in fine-tuned models by shifting the original model features along shift vectors. In addition, we find that the features related to different concepts are almost linearly separable (Fig. 11), and this becomes more prominent in deeper layers. This validates the linear representation hypothesis for MLLMs, previously studied for LLMs [32, 38]. Finally, model steering might be an alternative method to avoid costly fine-tuning.

5.1. Multimodal LLMs steering framework.

Setup. For a text-generative multimodal model $f : T \times I \rightarrow T$, we aim to modify the model’s output \hat{y} to a desired

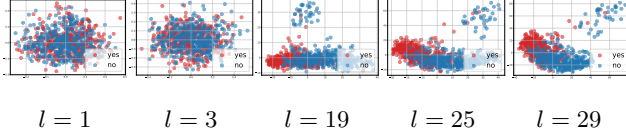


Figure 11. **Linear separability of concepts features in MLLMs.** We visualize the features related to the concepts "yes" and "no" after PCA projections across MLLMs layers.

output \tilde{y} by applying a shift or steering vector v to the residual stream features Z , without changing the model parameters. The model is evaluated within a visual question-answering (VQA) framework: where each query consists of a question about an input image, and the model generates an answer. This task encompasses a wide range of applications for MLLMs. To measure the effectiveness of our approach in directing the model towards specific answers or answer types, we report the number of generated answers that align with the target output or answer type. Additionally, we aim for targeted steering, ensuring that only specific answer types are influenced. For example, when altering answers from "yes" to "no" within the "yes/no" category, responses to other question types should remain unaffected. This specificity is assessed by monitoring accuracy across answer types and tracking the number of answers from each answer type.

Implementation details. Experiments are conducted on the widely-used LLaVA model [30], comprising a CLIP image encoder, a two-layer MLP connector, and a 7B Vicuna-1.5 LLM. In the main paper, we focus on VQAv2 dataset [18], a visual question-answering corpus with image-question-answer triplets and annotated answer types ("yes/no", "number", and "other"). We provide also experiments on COCO captioning [29], which we detail more in App. B. Steering vectors are derived from a subset of the training set, with model performance evaluated on the validation set. Additional experiments and ablation study can be found in App. B. We find that the steering becomes more effective in deeper layers (see Fig. 11 and App. B), thus we apply it on the last layer for VQAv2.

Target Type	Answers Type		
	yes/no	number	other
N/A	366	122	494
yes/no	557	96	288
number	327	201	390
other	364	115	501

Table 1. **Steering MLLMs answers type.** Number of target answers type increases significantly after steering the model with the corresponding steering vector.

5.2. Coarse-grained model steering

In coarse-grained or global steering, the objective is to adjust the model outputs \hat{y} to generally align with a set of target samples (*e.g.*, changing answers type). Given input-output samples, we first extract the answer representations $B = b_1, \dots, b_N$ at a specified layer l (we drop the layer index for simplicity) from the target sample set. Similarly, we obtain representations for a set of original samples $A = a_1, \dots, a_M$, for example, randomly drawn from the training set. We then compute the coarse steering vector s_c as follows:

$$s_c = \frac{\sum_i^N b_i}{N} - \frac{\sum_i^M a_i}{M}, \quad (7)$$

s_c is applied to all the samples in the validation set. For instance, the activations z_i of a sample x_i (at the same layer l), are changed as follows:

$$\tilde{z}_i = z_i + \alpha s_c, \quad z_i = f_l(x_i), \quad (8)$$

where α controls the steering strength and it is set to 1 (we study α in App. B). \tilde{z} , replaces z and becomes the input to the next layer $l + 1$.

Experiments. We steer the model answers towards a particular type among: yes/no, numbers or other (*e.g.* colors, objects). For each target answer type, we compute a steering vector. Table 1 shows that the number of answer types increases significantly when applying the corresponding steering vector, this validates the efficacy of globally steering the model.

5.3. Discovering meaningful and fine-grained steering directions.

Unlike global steering, fine-grained steering focuses on adjusting outputs at the concept level. Specifically, we seek editing directions that adjust only certain concepts. To do this, we decompose the hidden states of a set of samples into a set of concepts U . We then compute a series of fine-grained steering vectors $s^f = s_{11}^f, \dots, s_{NN}^f$, where each s_{ij}^f represents the steering vector from concept u_i to u_j :

$$s_{ij}^f = u_j - u_i. \quad (9)$$

However, not all computed vectors are necessarily meaningful steering vectors. We identify these vectors based on the strongest impact on guiding the model towards generating specific answers or concepts (*e.g.* producing significantly more target answers). This is more detailed in App. B.

Experiments. Fig. 12 illustrates some steering vectors. We try to find the steering vectors between concepts decomposed from 3 sample sets corresponding to: "yes/no", "number"

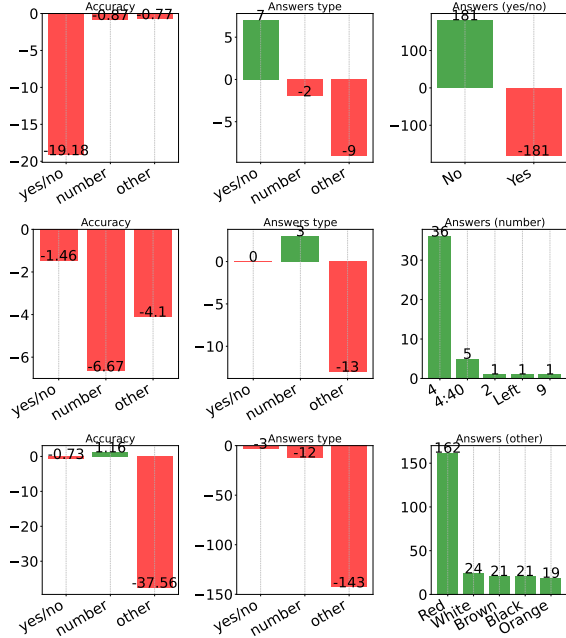


Figure 12. **Discovering meaningful steering directions.** Each line corresponds to a fine-grained steering direction to steer the model answer to: "No" (yes/no), "4" (number) and "Red" (other). Some steering directions are targeted (e.g., "No") as there is slight change in both the accuracy on other types (e.g., number, other) and the number of answers type. We show the relative scores compared to a baseline with no steering.

and "other" answers type. We notice that some vectors correspond to answering "No", "4" and "Red". This validates the possibility of finding fine-grained steering vectors that can steer the model towards a specific answer.

Steering	Accuracy (%)			Answer Types			Answers	
	Yes/No	Number	Other	Yes/No	Number	Other	Original	Target
N/A	90.82	58.47	71.10	1861	687	2349	0	0
Yes → No	69.03	56.82	68.99	1884	695	2294	-828	+828
1 → 3	90.71	54.52	71.12	1861	670	2350	-215	+144
White → Black	90.40	58.42	58.36	1861	671	2312	-98	+441

Table 2. **Steering MLLMs answers.** Steering answers from "Yes" (Yes/No), "1" (Number), "White" (Other) to "No", "3", "Black" respectively. The number of original/target answer counts decreases/increases significantly, while the accuracy on other answer types changes slightly, and the number of answer type counts remains almost constant.

5.4. Steering towards a specific target answer

Motivated by the previous section, the objective here is to steer the model towards a specific answer specified by the user. For each pair of original/target answers (e.g., yes/no), we collect few hundred samples and compute the steering vector (as in Section 5.2). Then we apply the vectors on all samples in the validation set. In Table 2, we report the evaluation metrics when targeting the last layer. We can

notice that the steering is effective as the number of target answers increase, while the accuracy on other answer types only slightly changes.

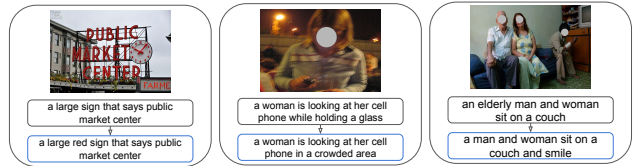


Figure 13. **Steering MLLMs captions style.** Captions steered to focus more on colors (left), places (middle) and sentiments (right).

5.5. Steering image captions

In our earlier experiments, we applied steering on relatively brief answers from the VQAv2 dataset. Here, we extend this approach to longer, descriptive outputs using the COCO image captioning dataset [29]. Given that multiple captions can effectively describe an image by emphasizing various aspects such as the main object, surroundings, actions, or events, our focus is modifying captions to align with a specific target style (see Fig. 13). We present the results in Table 3, demonstrating that captions can be steered towards a target style so that they focus more on places, colors, or sentiments. These findings validate the feasibility of steering MLLMs on tasks with longer responses.

Target Style	Captions Style		
	places	colors	sentiments
N/A	430	1309	2
places	796	1077	1
colors	488	2561	1
sentiments	393	1040	48

Table 3. **Steering MLLMs captions style.** Each line corresponds to different steering vector. Steering towards a target style increases the number of captions with that style.

6. Discussion

Limitations. Ideally, steering should be targeted; shifting from a "yes" to a "no" should affect only questions initially answered with "yes". While this is often achieved, it is not perfect. We also notice a tradeoff between the steering strength and the quality of generated responses. This approach focuses on changing the model answers or style, however, it can be extended to other applications, such as addressing biases or mitigating safety concerns. It is also interesting to extend our study to larger and more recent MLLMs, eventually with different architectures.

Conclusion. Gaining insights into the mechanisms of recent foundation models is crucial for advancing AI research. In this study, we delve into how MLLMs’ internal representations evolve during fine-tuning, demonstrating that concepts learned post-fine-tuning can often be recovered from the original model by navigating the feature space. This approach inspired our final investigation, where we steer model behavior by modifying features directly, without additional training. We show that this could be used to change model answers, or have richer captions focusing on different aspects of the image. We hope this work motivates further research into understanding these models and developing more efficient methods for adapting or refining them, moving beyond traditional training practices.

References

- [1] Jean-Baptiste Alayrac, Jeff Donahue, Pauline Luc, Antoine Miech, Iain Barr, Yana Hasson, Karel Lenc, Arthur Mensch, Katherine Millican, Malcolm Reynolds, et al. Flamingo: a visual language model for few-shot learning. *Advances in Neural Information Processing Systems*, 35:23716–23736, 2022. 1
- [2] Andy Arditi, Oscar Obeso, Aaqib Syed, Daniel Paleka, Nina Rimsky, Wes Gurnee, and Neel Nanda. Refusal in language models is mediated by a single direction. *arXiv preprint arXiv:2406.11717*, 2024. 2
- [3] Jinze Bai, Shuai Bai, Shusheng Yang, Shijie Wang, Sinan Tan, Peng Wang, Junyang Lin, Chang Zhou, and Jingren Zhou. Qwen-vl: A frontier large vision-language model with versatile abilities. *arXiv preprint arXiv:2308.12966*, 2023. 1, 2
- [4] Folco Bertini Baldassini, Mustafa Shukor, Matthieu Cord, Laure Soulier, and Benjamin Piwowarski. What makes multimodal in-context learning work? In *Proceedings of the IEEE/CVF Conference on Computer Vision and Pattern Recognition (CVPR) Workshops*, pages 1539–1550, June 2024. 1, 2
- [5] Nora Belrose, Zach Furman, Logan Smith, Danny Halawi, Igor V. Ostrovsky, Lev McKinney, Stella Biderman, and Jacob Steinhardt. Eliciting latent predictions from transformers with the tuned lens. *ArXiv*, abs/2303.08112, 2023. 3
- [6] Nora Belrose, David Schneider-Joseph, Shauli Ravfogel, Ryan Cotterell, Edward Raff, and Stella Biderman. Leace: Perfect linear concept erasure in closed form. *Advances in Neural Information Processing Systems*, 36, 2024. 2
- [7] Tom Brown, Benjamin Mann, Nick Ryder, Melanie Subbiah, Jared D Kaplan, Prafulla Dhariwal, Arvind Neelakantan, Pranav Shyam, Girish Sastry, Amanda Askell, et al. Language models are few-shot learners. *Advances in Neural Information Processing Systems (NeurIPS)*, 33:1877–1901, 2020. 1
- [8] Shuo Chen, Zhen Han, Bailan He, Mark Buckley, Philip Torr, Volker Tresp, and Jindong Gu. Understanding and improving in-context learning on vision-language models. In *ICLR 2024 Workshop on Mathematical and Empirical Understanding of Foundation Models*, 2024. 2
- [9] Shi Chen and Qi Zhao. Rex: Reasoning-aware and grounded explanation. In *Proceedings of the IEEE/CVF Conference on Computer Vision and Pattern Recognition*, pages 15586–15595, 2022. 2
- [10] Aakanksha Chowdhery, Sharan Narang, Jacob Devlin, Maarten Bosma, Gaurav Mishra, Adam Roberts, Paul Barham, Hyung Won Chung, Charles Sutton, Sebastian Gehrmann, et al. Palm: Scaling language modeling with pathways. *arXiv preprint arXiv:2204.02311*, 2022. 1
- [11] Danny Driess, Fei Xia, Mehdi SM Sajjadi, Corey Lynch, Aakanksha Chowdhery, Brian Ichter, Ayzan Wahid, Jonathan Tompson, Quan Vuong, Tianhe Yu, et al. Palm-e: An embodied multimodal language model. *arXiv preprint arXiv:2303.03378*, 2023. 1
- [12] Nelson Elhage, Neel Nanda, Catherine Olsson, Tom Henighan, Nicholas Joseph, Ben Mann, Amanda Askell, Yuntao Bai, Anna Chen, Tom Conerly, et al. A mathematical framework for transformer circuits. *Transformer Circuits Thread*, 1, 2021. 3, 12
- [13] Thomas Fel, Victor Boutin, Louis Béthune, Rémi Cadène, Mazda Moayeri, Léo Andéol, Mathieu Chalvidal, and Thomas Serre. A holistic approach to unifying automatic concept extraction and concept importance estimation. *Advances in Neural Information Processing Systems*, 36, 2023. 2
- [14] Thomas Fel, Agustin Picard, Louis Bethune, Thibaut Boissin, David Vigouroux, Julien Colin, Rémi Cadène, and Thomas Serre. Craft: Concept recursive activation factorization for explainability. In *Proceedings of the IEEE/CVF Conference on Computer Vision and Pattern Recognition*, pages 2711–2721, 2023. 2
- [15] Enrico Fini, Mustafa Shukor, Xiujun Li, Philipp Dufter, Michal Klein, David Haldimann, Sai Aitharaju, Victor Guilherme Turrissi da Costa, Louis Béthune, Zhe Gan, et al. Multimodal autoregressive pre-training of large vision encoders. *arXiv preprint arXiv:2411.14402*, 2024. 2
- [16] Jiaxin Ge, Sanjay Subramanian, Trevor Darrell, and Boyi Li. From wrong to right: A recursive approach towards vision-language explanation. In *Proceedings of the 2023 Conference on Empirical Methods in Natural Language Processing*, pages 1173–1185, 2023. 2
- [17] Amirata Ghorbani, James Wexler, James Y Zou, and Been Kim. Towards automatic concept-based explanations. In *Advances in Neural Information Processing Systems (NeurIPS)*, pages 9277–9286, 2019. 2
- [18] Yash Goyal, Tejas Khot, Douglas Summers-Stay, Dhruv Batra, and Devi Parikh. Making the v in vqa matter: Elevating the role of image understanding in visual question answering. In *Proceedings of the IEEE conference on computer vision and pattern recognition*, pages 6904–6913, 2017. 7, 13
- [19] J. Edward Hu, Yelong Shen, Phillip Wallis, Zeyuan Allen-Zhu, Yuanzhi Li, Shean Wang, and Weizhu Chen. Lora: Low-rank adaptation of large language models. *ArXiv*, abs/2106.09685, 2021. 3, 12
- [20] Kaichen Huang, Jiahao Huo, Yibo Yan, Kun Wang, Yutao Yue, and Xuming Hu. Miner: Mining the underlying pattern of modality-specific neurons in multimodal large language models. *arXiv preprint arXiv:2410.04819*, 2024. 2
- [21] Robert Huben, Hoagy Cunningham, Logan Riggs Smith, Aidan Ewart, and Lee Sharkey. Sparse autoencoders find

- highly interpretable features in language models. In *The Twelfth International Conference on Learning Representations*, 2024. 2
- [22] Albert Q Jiang, Alexandre Sablayrolles, Arthur Mensch, Chris Bamford, Devendra Singh Chaplot, Diego de las Casas, Florian Bressand, Gianna Lengyel, Guillaume Lample, Lucile Saulnier, et al. Mistral 7b. *arXiv preprint arXiv:2310.06825*, 2023. 1, 2
- [23] Been Kim, Martin Wattenberg, Justin Gilmer, Carrie Cai, James Wexler, Fernanda Viegas, et al. Interpretability beyond feature attribution: Quantitative testing with concept activation vectors (tcav). In *International conference on machine learning*, pages 2668–2677. PMLR, 2018. 2
- [24] Ranjay Krishna, Yuke Zhu, Oliver Groth, Justin Johnson, Kenji Hata, Joshua Kravitz, Stephanie Chen, Yannis Kalantidis, Li-Jia Li, David A. Shamma, Michael S. Bernstein, and Li Fei-Fei. Visual genome: Connecting language and vision using crowdsourced dense image annotations. *Int. J. Comput. Vis.*, 123(1):32–73, 2017. 4, 12
- [25] Anna Langedijk, Hosein Mohebbi, Gabriele Sarti, Willem Zuidema, and Jaap Jumelet. Decoderlens: Layerwise interpretation of encoder-decoder transformers. *ArXiv*, abs/2310.03686, 2023. 3
- [26] Hugo Laurençon, Lucile Saulnier, Léo Tronchon, Stas Bekman, Amanpreet Singh, Anton Lozhkov, Thomas Wang, Siddharth Karamcheti, Alexander Rush, Douwe Kiela, et al. Obelics: An open web-scale filtered dataset of interleaved image-text documents. *Advances in Neural Information Processing Systems*, 36, 2024. 1
- [27] Hugo Laurençon, Léo Tronchon, Matthieu Cord, and Victor Sanh. What matters when building vision-language models? *arXiv preprint arXiv:2405.02246*, 2024. 1, 2, 3
- [28] Kenneth Li, Oam Patel, Fernanda Viégas, Hanspeter Pfister, and Martin Wattenberg. Inference-time intervention: Eliciting truthful answers from a language model. *Advances in Neural Information Processing Systems*, 36, 2024. 2
- [29] Tsung-Yi Lin, Michael Maire, Serge Belongie, James Hays, Pietro Perona, Deva Ramanan, Piotr Dollár, and C Lawrence Zitnick. Microsoft coco: Common objects in context. In *Computer Vision—ECCV 2014: 13th European Conference, Zurich, Switzerland, September 6–12, 2014, Proceedings, Part V 13*, pages 740–755. Springer, 2014. 7, 8, 12, 14
- [30] Haotian Liu, Chunyuan Li, Yuheng Li, and Yong Jae Lee. Improved baselines with visual instruction tuning. In *Proceedings of the IEEE/CVF Conference on Computer Vision and Pattern Recognition*, pages 26296–26306, 2024. 1, 2, 3, 7, 12, 13
- [31] Oscar Mañas, Pau Rodriguez Lopez, Saba Ahmadi, Aida Nematzadeh, Yash Goyal, and Aishwarya Agrawal. Mapl: Parameter-efficient adaptation of unimodal pre-trained models for vision-language few-shot prompting. In *Proceedings of the 17th Conference of the European Chapter of the Association for Computational Linguistics*, pages 2523–2548, 2023. 1
- [32] Neel Nanda. Actually, othello-gpt has a linear emergent world model, Mar 2023. 6, 18
- [33] Nostalgebraist. Interpreting gpt: The logit lens. <https://www.lesswrong.com/posts/AcKRB8wDpdaN6v6ru/interpreting-gpt-the-logit-lens>, 2020. Accessed: [date of access]. 3
- [34] OpenAI. Gpt-4 technical report. *arXiv*, 2023. 1
- [35] Haowen Pan, Yixin Cao, Xiaozhi Wang, and Xun Yang. Finding and editing multi-modal neurons in pre-trained transformer. *arXiv preprint arXiv:2311.07470*, 2023. 2
- [36] Nina Panickssery, Nick Gabrieli, Julian Schulz, Meg Tong, Evan Hubinger, and Alexander Matt Turner. Steering llama 2 via contrastive activation addition. *arXiv preprint arXiv:2312.06681*, 2023. 2
- [37] Jayneel Parekh, Pegah Khayatan, Mustafa Shukor, Alasdair Newson, and Matthieu Cord. A concept-based explainability framework for large multimodal models. In *Advances in Neural Information Processing Systems (NeurIPS)*, 2024. 1, 2, 3, 12
- [38] Kiho Park, Yo Joong Choe, and Victor Veitch. The linear representation hypothesis and the geometry of large language models. In *Forty-first International Conference on Machine Learning*, 2024. 6, 18
- [39] Libo Qin, Qiguang Chen, Hao Fei, Zhi Chen, Min Li, and Wanxiang Che. What factors affect multi-modal in-context learning? an in-depth exploration. *arXiv preprint arXiv:2410.20482*, 2024. 2
- [40] Alec Radford, Jong Wook Kim, Chris Hallacy, Aditya Ramesh, Gabriel Goh, Sandhini Agarwal, Girish Sastry, Amanda Askell, Pamela Mishkin, Jack Clark, et al. Learning transferable visual models from natural language supervision. In *International conference on machine learning*, pages 8748–8763. PMLR, 2021. 2, 4
- [41] Senthoran Rajamanoharan, Arthur Conmy, Lewis Smith, Tom Lieberum, Vikrant Varma, János Kramár, Rohin Shah, and Neel Nanda. Improving dictionary learning with gated sparse autoencoders. In *Advances in Neural Information Processing Systems*, 2024. 2
- [42] Shauli Ravfogel, Michael Twiton, Yoav Goldberg, and Ryan D Cotterell. Linear adversarial concept erasure. In *International Conference on Machine Learning*, pages 18400–18421. PMLR, 2022. 2
- [43] Mansi Sakarvadia, Arham Khan, Aswathy Ajith, Daniel Grzenda, Nathaniel Hudson, André Bauer, Kyle Chard, and Ian T. Foster. Attention lens: A tool for mechanistically interpreting the attention head information retrieval mechanism. *CoRR*, abs/2310.16270, 2023. 3
- [44] Sarah Schwettmann, Neil Chowdhury, Samuel Klein, David Bau, and Antonio Torralba. Multimodal neurons in pretrained text-only transformers. In *Proceedings of the IEEE/CVF International Conference on Computer Vision*, pages 2862–2867, 2023. 1, 2
- [45] Mustafa Shukor and Matthieu Cord. Implicit multimodal alignment: On the generalization of frozen llms to multimodal inputs. *Advances in Neural Information Processing Systems (NeurIPS)*, 2024. 1, 2, 12
- [46] Mustafa Shukor and Matthieu Cord. Skipping computations in multimodal llms. *arXiv preprint arXiv:2410.09454*, 2024. 1
- [47] Mustafa Shukor, Corentin Dancette, and Matthieu Cord. epalm: Efficient perceptual augmentation of language models. In *Proceedings of the IEEE/CVF International Conference on Computer Vision*, pages 22056–22069, 2023. 1
- [48] Mustafa Shukor, Alexandre Rame, Corentin Dancette, and

- Matthieu Cord. Beyond task performance: evaluating and reducing the flaws of large multimodal models with in-context-learning. In *The Twelfth International Conference on Learning Representations*, 2024. 1, 2
- [49] Nishant Subramani, Nivedita Suresh, and Matthew E Peters. Extracting latent steering vectors from pretrained language models. In *Findings of the Association for Computational Linguistics: ACL 2022*, pages 566–581, 2022. 2
- [50] Gemma Team, Morgane Riviere, Shreya Pathak, Pier Giuseppe Sessa, Cassidy Hardin, Surya Bhupatiraju, Léonard Hussenot, Thomas Mesnard, Bobak Shahriari, Alexandre Ramé, et al. Gemma 2: Improving open language models at a practical size. *arXiv preprint arXiv:2408.00118*, 2024. 2
- [51] Curt Tigges, Oskar John Hollinsworth, Atticus Geiger, and Neel Nanda. Linear representations of sentiment in large language models. *arXiv preprint arXiv:2310.15154*, 2023. 2
- [52] Hugo Touvron, Louis Martin, Kevin Stone, Peter Albert, Amjad Almahairi, Yasmine Babaei, Nikolay Bashlykov, Soumya Batra, Prajjwal Bhargava, Shruti Bhosale, et al. Llama 2: Open foundation and fine-tuned chat models. *arXiv preprint arXiv:2307.09288*, 2023. 1, 2
- [53] Alexander Matt Turner, Lisa Thiergart, Gavin Leech, David Udell, Juan J Vazquez, Ulisse Mini, and Monte MacDiarmid. Activation addition: Steering language models without optimization. *arXiv preprint arXiv:2308.10248*, 2023. 2
- [54] Théophile Vallaeys, Mustafa Shukor, Matthieu Cord, and Jakob Verbeek. Improved baselines for data-efficient perceptual augmentation of llms. *arXiv preprint arXiv:2403.13499*, 2024. 1, 2, 12
- [55] Zhengxuan Wu, Aryaman Arora, Zheng Wang, Atticus Geiger, Dan Jurafsky, Christopher D Manning, and Christopher Potts. Refit: Representation finetuning for language models. *arXiv preprint arXiv:2404.03592*, 2024. 2
- [56] Dizhan Xue, Shengsheng Qian, and Changsheng Xu. Few-shot multimodal explanation for visual question answering. In *ACM Multimedia 2024*, 2024. 2
- [57] Chih-Kuan Yeh, Been Kim, Sercan O Arik, Chun-Liang Li, Pradeep Ravikumar, and Tomas Pfister. On concept-based explanations in deep neural networks. *arXiv preprint arXiv:1910.07969*, 2019. 2
- [58] Xiaohua Zhai, Basil Mustafa, Alexander Kolesnikov, and Lucas Beyer. Sigmoid loss for language image pre-training. In *Proceedings of the IEEE/CVF International Conference on Computer Vision*, pages 11975–11986, 2023. 2
- [59] Susan Zhang, Stephen Roller, Naman Goyal, Mikel Artetxe, Moya Chen, Shuohui Chen, Christopher Dewan, Mona T. Diab, Xian Li, Xi Victoria Lin, Todor Mihaylov, Myle Ott, Sam Shleifer, Kurt Shuster, Daniel Simig, Punit Singh Koura, Anjali Sridhar, Tianlu Wang, and Luke Zettlemoyer. Opt: Open pre-trained transformer language models. *ArXiv*, abs/2205.01068, 2022. 4
- [60] Xiaofeng Zhang, Chen Shen, Xiaosong Yuan, Shaotian Yan, Liang Xie, Wenxiao Wang, Chaochen Gu, Hao Tang, and Jieping Ye. From redundancy to relevance: Enhancing explainability in multimodal large language models. *arXiv preprint arXiv:2406.06579*, 2024. 1

Analyzing Fine-tuning Representation Shift for Multimodal LLMs Steering alignment

Supplementary material

This supplementary material is organized as follows:

- App. A provides details on the notations and implementation related to the analysis of representation shift presented in the main paper, and further expands on the previous analysis.
- App. B details the implementation for steering the model, as introduced in the main paper. It further extends the analysis with ablation studies and qualitative results.

The code for this project is publicly available at <https://github.com/mshukor/xl-vlms>.

A. Fine-tuning and evolution of concept representations

This section provides additional details and analyses on the evolution of concepts due to fine-tuning and their recovery using shift vectors. App. A.1 introduces additional notations. App. A.2 describes our experiments’ models, fine-tuning setup, and datasets. App. A.3 analyzes the change of concepts during training. In App. A.4.2, we present ablation studies related to concepts recovery. App. A.5 discusses the correlation between the concepts recovery and the consistency of their shifts. Finally, App. A.6 covers experiments conducted with the LLaVA-1.5 [30].

A.1. Notations

Additional Details on the Residual Stream View In the main paper, we focus on the representation in the residual stream. Similar to [12], this can be expressed as follows:

$$h_{(l+1)}^p = h_{(l)}^p + a_{(l)}^p + m_{(l)}^p,$$

$a_{(l)}^p$ is computed from $h_{(l)}^1, \dots, h_{(l)}^p$, by the attention mechanism at layer l and position p . $m_{(l)}^p$ represents the output of the MLP block which operates on $h_{(l)}^p + a_{(l)}^p$.

Bijjective matching. To compute the bijjective matching between concepts from two models, we first compute the cosine similarity between $U^a = \{\mathbf{u}_1^a, \mathbf{u}_2^a, \dots, \mathbf{u}_K^a\}$ and $U^b = \{\mathbf{u}_1^b, \mathbf{u}_2^b, \dots, \mathbf{u}_K^b\}$, represented as $S \in \mathbb{R}^{K \times K}$, where:

$$S_{ij} = \frac{\mathbf{u}_i^a \cdot \mathbf{u}_j^b}{\|\mathbf{u}_i^a\| \|\mathbf{u}_j^b\|}.$$

Next, we use an optimal transport approach to find the association that optimizes the overall matching cost. Defining a transport plan $\gamma \in \mathbb{R}^{K \times K}$, we solve the optimal transport problem to minimize the cost $\min_{\gamma} \sum_{i,j} \gamma_{ij} \cdot (1 - S_{ij})$ subject to the constraints $\gamma \mathbf{1} = \mathbf{1}$, $\gamma^T \mathbf{1} = \mathbf{1}$, and $\gamma_{ij} \in \{0, 1\}$. Here, each entry γ_{ij} indicates the matching state of the concepts \mathbf{u}_i^a and \mathbf{u}_j^b .

A.2. Implementation details

Our analysis spans MLLMs following the architecture detailed in the paper. We distinguish 2 setups; single-task tuning that covers most of the analysis part in the main paper, and multi-task tuning with additional results in the appendix. For multi-task setup, we use LLaVA [30], that consists of a CLIP image encoder, a two-layer MLP connector, and a 7B Vicuna-1.5 LLM. For single-task setup, we follow the setup in [37, 45, 54].

We fine-tune the LLM with Low-Rank Adaptation (LoRA) [19], which modifies the weight matrices of the model with a low-rank update. We use AdamW optimizer with a weight decay of 0.01 and choose the learning rate and LoRA rank that works best for each fine-tuning dataset. For LLaVA, we follow the hyperparameters recommended by the authors, including the rank $r = 128$ and learning rate $2e-4$.

We fine-tune the models using three distinct subsets of Visual Genome (VG) dataset [24]: *color*, *sentiment*, and *place*. These subsets respectively correspond to about $21k$ samples describing colors, $5k$ samples containing sentiments and $27k$ samples that describe the locations or environments. All subsets were curated based on keyword occurrences provided in Fig. 15. We also use COCO captioning dataset [29] for hidden states extraction, throughout the quantitative experiments. Different than VG, COCO contains captions describing the image general, often focusing on the central object.

A.3. Concepts change during training

In this section, we show how fine-tuning deviates the fine-tuned concepts compared to the original ones.

To this end, we analyze the cosine similarity and text grounding overlap (T-Overlap) for each concept across training epochs and subsets. Specifically, we examine the cosine similarity and word overlap between an original concept \mathbf{u}_i^a and its closest match $m(i)$ in the fine-tuned model at various stages of fine-tuning, where $m(i)$ is defined as:

$$m(i) = \arg \max_{\mathbf{u}_j^b \in U^b} \cos(\mathbf{u}_i^a, \mathbf{u}_j^b)$$

Fig. 14 shows that both the cosine similarity and text overlap plots exhibit a consistent decreasing trend throughout fine-tuning, indicating that the model deviates further from the original concepts as training progresses.

In the per-concept plot, we observe that the fine-tuning process affects each *dog*-related concept differently, demonstrating various levels of change across concepts. Notably, concepts 0 and 10, which are related to *hot dogs* rather than *dogs*, exhibit a relatively smaller drift, suggesting that the fine-tuning process impacts different concepts with varying magnitudes. These results further support our observation that fine-tuning leads to a systematic deviation from the original model’s representations, though the extent of this drift varies between concepts.

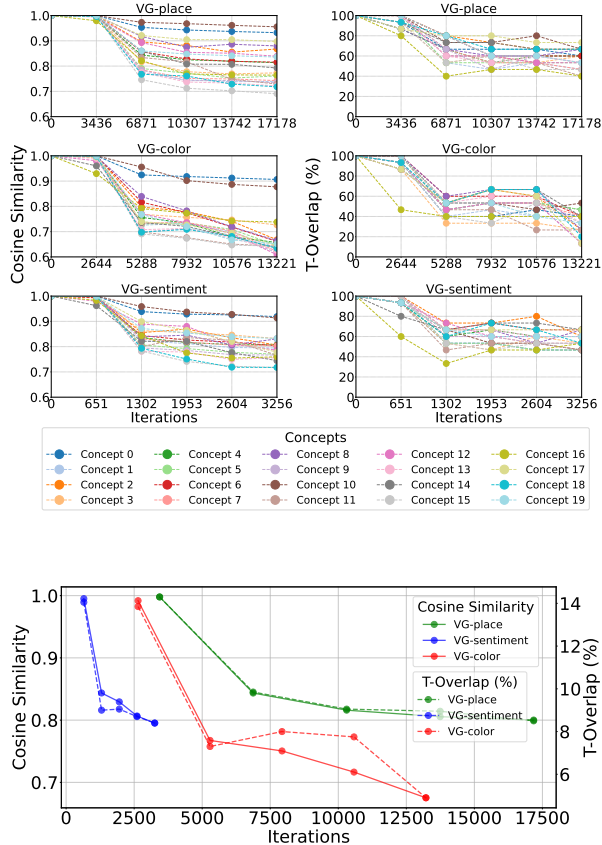


Figure 14. **Concepts change during training.** Illustration of the similarity between the original concepts the concepts during fine-tuning. Top: individual concepts change. Bottom: average concepts change.

A.4. Concepts recovery and shift vectors

A.4.1 Concepts specialization to the fine-tuning task

We investigate the relationship between the shift vectors effect and the fine-tuning task. We vary α and report the average (average over $K = 20$ concepts) overlap between the text grounding of the shifted concept \mathbf{u}_k^s and the set of keywords $\{w_1, \dots, w_m\} \subset \mathcal{Y}$ associated with the fine-tuning task (Sec. 3). Fig. 16 shows that the shift vectors move the original clusters to be more related to the task keywords.

A.4.2 Ablation study

In the following, we present ablation studies to different design choices.

Number of concepts and recovery. We investigate the effect of varying the number of concepts K on the recovery. We report the T-Overlap between the fine-tuned model concepts and their match (matching is bijective as in App. A.1), both in the shifted \mathbf{u}_k^s and the original concepts \mathbf{u}_k^a . Fig. 17 shows that the number of concepts does not significantly influence the concept recovery.

Concepts recovery across layers. We investigate the effect of varying the layer from which we extract the concepts. We report the average and the maximum of T-Overlap. Fig. 18 shows that the gap between the T-Overlap with shifted and T-Overlap with original concepts is higher in deeper layers, indicating better recovery.

A.5. Concepts shift consistency and magnitude

Each concept shift vector $\Delta_k^{a \rightarrow b}(\mathbf{u}_k^a)$ is computed from a set of individual sample representation shifts $\{\delta_m\}_{m \in A_k}$. We hypothesize, that if the individual shifts are consistent (*i.e.*, move in a single direction), the concept shift vector has a higher magnitude, which is highly correlated with the recovery of concepts. To this end, we quantify the consistency by computing the mean cosine similarity of individual representation shifts with the concept shift vector. This can be expressed using the cosine similarity between each vector δ_m and the mean vector $\Delta_k^{a \rightarrow b}(\mathbf{u}_k^a)$:

$$\text{Consistency}(\mathbf{u}_k^a) = \frac{1}{|A_k|} \sum_{m \in A_k} \cos(\delta_m, \Delta_k^{a \rightarrow b}(\mathbf{u}_k^a)),$$

We corroborate our hypothesis by plotting the variation of concept shift vector magnitudes with the consistency of their shifts for concepts related to animal dog in App. A.5. Beyond the established correlation, the average magnitude of individual shifts δ_m remain similar across concepts (48.06 ± 3.887 , 57.6 ± 1.796 , and 47.9 ± 3.96)— where the values represent the mean and standard deviation for animal dog concepts for different finetuning tasks. This suggests that a higher consistency is linked to a larger magnitude of the mean shift vector, indicating that individual shifts are more aligned and do not cancel each other out.

We provide additional results using LLaVA model in Fig. 21.

A.6. Additional experiments with LLaVA model

In this section, we extend our main experiments to the LLaVA model, adhering to the same experimental setup as described previously. We report the text grounding recovery evaluation in Fig. 20 and the relationship between shift metrics and the recovery in Fig. 21, providing further insights into the consistency and generalizability of our findings across different models.

B. Fine-grained multimodal LLM steering

This section provides additional results and details about model steering. Specifically, implementation details App. B.1, discovering steering directions towards single or multiple concepts App. B.3, steering image captions App. B.4, ablation study for the steering layer, number of samples and the steering strength App. B.5, more visualization related to the linear separability of concepts App. B.6, and finally, some qualitative results App. B.7.

B.1. Implementation details

Experiments are conducted on the widely-used LLaVA model [30], comprising a CLIP image encoder, a two-layer MLP connector, and a 7B Vicuna-1.5 LLM. In the main paper, we focus on VQA v2 dataset [18], a visual question-answering corpus with image-question-answer triplets and annotated answer types ("yes/no", "number", and "other"). We provide also experiments on

beach, mountain, forest, desert, city, village, river, ocean, park, island, countryside, jungle, cave, waterfall, lake, garden, market, museum, restaurant, airport, street, cinema, theater, school, library, stadium, bridge, station, bus stop, hotel, zoo, church, temple, mall, hospital, playground, harbor, factory, tower, university

red, blue, green, yellow, orange, purple, pink, brown, black, white, gray, cyan, magenta, turquoise, indigo, maroon, beige, gold, silver, olive, lavender, navy, teal, peach, violet, ivory, charcoal, amber, emerald, coral

tranquil, elated, proud, love, grumpy, emotion, identity, thoughtful, bewildered, upset, optimistic, serene, relief, hope, delighted, melancholy, serious, content, disgust, solitude, facial expression, pleased, grin, determined, weakness, playful, introspective, reluctant, imaginative, sad, dream, disappointed, reality, hate, anxious, nightmare, laugh, freedom, nervous, worried, powerful, inspiration, ashamed, frown, blushing, solitary, realistic, tears, fearless, happy, confusion, pensive, skeptical, lonely, triumphant, mystery, alienation, hopeful, concentration, faith, weak, destiny, frustrated, conflict, acceptance, wise, mysterious, emptiness, smirk, contentment, chaotic, wisdom, connection, purpose, free, relaxed, bored, doubtful, mournful, purposeful, excited, fear, trust, imagination, anger, fate, joy, awkward, accepting, insecure, crying, amused, intense, memory, inspirational, doubt, faithful, jealous, illusion, smile, ecstatic, surprised, identifiable, curious, gloomy, cheerful, chaos

Figure 15. **VG subsets.** Keywords used to extract VG subsets. Each subset is selected based on the presence of the corresponding words in the captions. From top to bottom, words related to: places, colors, and sentiments.

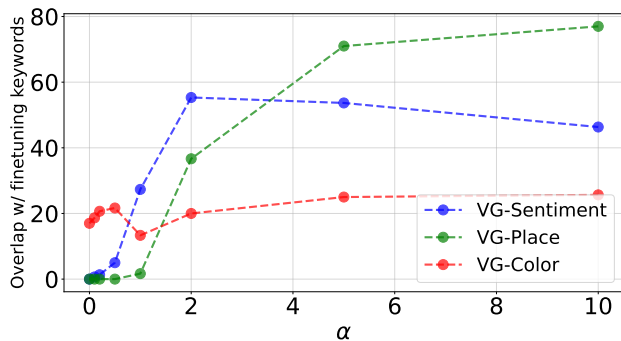


Figure 16. **Concepts specialization to the fine-tuning task.** Illustration of the mean intersection between the text grounding of shifted concepts (with magnitude α) and the keywords associated with different fine-tuning datasets (with TOI ‘Dog’). $\alpha = 0$ corresponds to the original model.

COCO captioning [29], that contains images and captions describing them. Because COCO does not contain style annotations, we automatically annotate the dataset. Specifically, for each style (*e.g.*, colors, places, sentiments) if any of the descriptive keywords (*e.g.* red, blue, white ... for colors) is present in the caption, we consider it belonging to the corresponding style. Steering vectors are derived from a subset of the training set, with model performance evaluated on the validation set. We only use few hundred examples to compute the steering vectors, as we find this design choice does not have a significant effect on the final results (App. B.5.1). We did

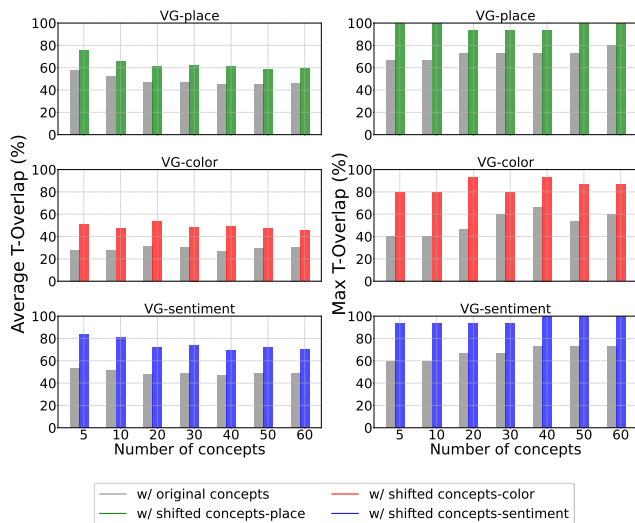
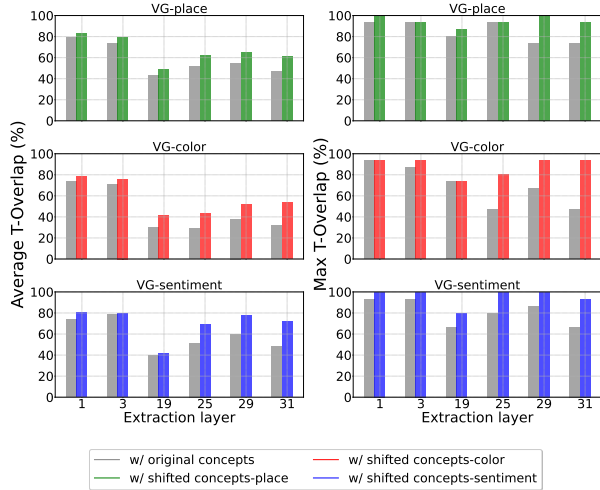


Figure 17. **Concepts extraction layer and recovery.** We investigate the impact of shifting concepts extracted from different layers, and evaluate their recovery. The results show that the recovery improves with deeper layers, as the gap between the T-Overlap with original and with shifted concepts becomes larger.

an ablation over the which layer to apply the steering and select the best layer based on an evaluation on a validation set (App. B.5.2). Specifically, for VQAv2 we find the last layer works best, while for COCO the 20th layer is best. We report the evaluation metrics (*e.g.*



(a)

Figure 18. **Number of concepts and recovery.** Varying the number of concepts K has minimal impact on the recovery, as measured by the overlap metrics, indicating the robustness of the recovery process to the choice of K .

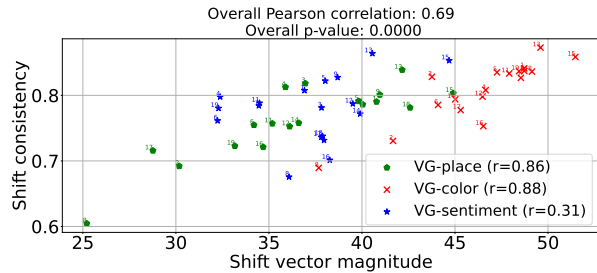


Figure 19. **Correlation between the shift vector magnitude and the shift consistency.** Each point corresponds to a concept fine-tuned on 3 VG subsets. The higher the shift vector magnitude, the higher the shift consistency (as defined in App. A.5)

accuracy, CIDEr) on 5k and 3k random samples for VQAv2 and COCO respectively.

B.2. Steering other MLLMs

B.3. Discovering meaningful steering directions.

Steering vectors selection metric. Not all computed vectors are necessarily meaningful steering vectors. We identify those that are meaningful, as those with the strongest impact on guiding the model towards generating specific answers or concepts. The selection process follows these steps:

- For each steering vector in a set, apply it to steer the model’s behavior.
- Measure the change in the answers number of occurrence between the steered model and the original model, producing the count of relative occurrences for each answer.
- For each vector, keep the top N answers with the highest relative occurrence counts.
- Use k-means ($k=2$) to cluster the top N answers.

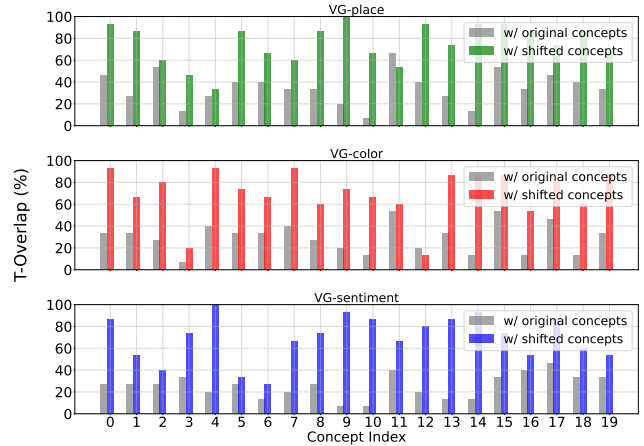


Figure 20. **Recovering fine-tuned LLaVA-1.5 model concepts.** For each matched fine-tuned concept we report its text grounding overlap with the original concept and the shifted concept. Model fine-tuned on: places (top), colors (middle) and sentiments (bottom).

- Assign each answer to one of the two clusters. The primary answers are those belonging to the cluster with the highest total occurrences. These answers are considered the target answers for the steering vector.
- Calculate the difference in relative occurrence between primary answers and those in the secondary cluster.
- Select the steering directions that exhibit the highest differences in relative occurrence between clusters. This is considered our selection score.

We use clustering to accommodate the possibility of steering multiple concepts at a time.

Steering directions towards a single concept. Following our selection process discussed previously, we illustrate some of the steering vectors that have the highest selection score. We decompose the clusters from 3 answers type: colors, numbers and other. Fig. 22 and Fig. 23 shows that the vectors corresponds to steering the model towards very specific answer, such as No, Red and 4.

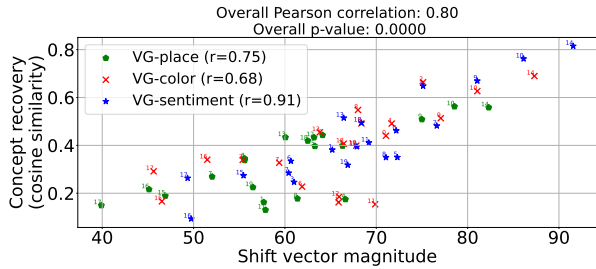
Steering directions towards multiple concepts. We can also find vectors that steer the model towards more than one answer, this is because some concepts might encompass different answers. Fig. 24 shows that some steering vectors corresponds to "3" and "4" or "Yellow" and "Orange".

B.4. Steering image captions.

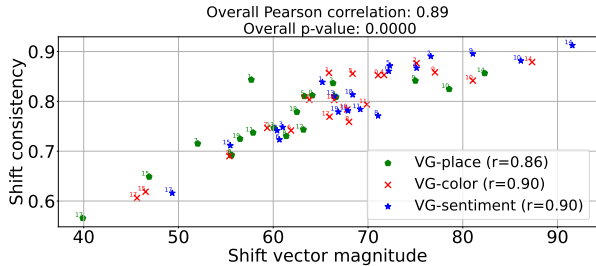
Similar to VQAv2, we extract the concepts from a set of image captions and compute the steering vectors between each pair of concepts. Fig. 25 illustrate some of these vectors. Based on the relative increase in words count, we can notice that some steering vectors are related to specific concepts, such as "holding" or "black". In addition, we find (Fig. 26) some vectors correspond to multiple concepts, such as "standing" and "sitting" or "young" and "group" and "large".

Model	Steering	Accuracy (%)			Answer Types			Answers	
		Yes/No	Number	Other	Yes/No	Number	Other	Original	Target
LLaVA-1.5	N/A	90.82	58.47	71.10	1861	687	2349	0	0
	Yes → No	69.03	56.82	68.99	1884	695	2294	-828	+828
	1 → 3	90.71	54.52	71.12	1861	670	2350	-215	+144
	White → Black	90.40	58.42	58.36	1861	671	2312	-98	+441
Qwen2-VL-Instruct	N/A	95.20	77.31	74.67	1861	676	2343	0	0
	Yes → No	64.96	58.37	40.83	3034	608	1176	-900	+901
	1 → 3	95.33	41.68	74.15	1859	671	2346	-187	+291
	White → Black	95.28	76.41	68.27	1863	683	2334	-92	+176
Idefics2	N/A	93.77	62.57	73.77	1851	657	2342	0	0
	Yes → No	64.96	61.47	62.24	2362	654	1807	-906	+907
	1 → 3	94.11	39.23	72.94	1850	668	2323	-104	+118
	White → Black	93.77	62.82	64.33	1855	659	2322	-95	+396

Table 4. **Steering MLLMs answers.** Steering answers from "Yes" (yes/no), "1" (number), "White" (other) to "No", "3", "Black" respectively. The number of original/target answer counts decrease/increase significantly, while the accuracy on other answer types changes slightly, and the number of answer type counts remains almost constant. Steering at layer: last (LLaVA-1.5), 23 (Qwen2-VL), 25 (Idefics2).



(a) **Correlation between shift vector magnitudes and concept recovery for LLaVA-1.5 model.** The higher the shift vector magnitude the better the concept recovery.



(b) **Correlation between the shift vector magnitude and shift consistency.** The higher the shift vector magnitude, the higher the shift consistency.

Figure 21. **Concepts recovery and shift consistency with LLaVA-1.5.** Each point corresponds to a concept from LLaVA-1.5 fine-tuned on 3 VG subsets. Beyond the established correlation, the similar magnitude of individual shifts across concepts (80.3 ± 7.086 , 84.1 ± 6.31 , and 85.6 ± 5.95)—where the values represent the mean and standard deviation of averaged individual shift magnitudes across animal dog concepts—suggests that a higher consistency is linked to a larger magnitude of the mean shift vector, indicating that individual shifts are more aligned and do not cancel each other out.

B.5. Ablation study

In this section, we ablate several steering design choices.

B.5.1 Number of samples

An interesting question to ask is how the steering is affected by the number of samples. To provide an answer, we vary the number of samples (*e.g.* answers with yes and no) used to compute the steering vectors and report the results in Fig. 27. Interestingly, the steering is effective even with very few samples (*e.g.*, 50) and it is robust to the number of samples, where the scores start to saturate after 500 samples. This reveals that steering could be a good data-efficient solution for setups with very little data.

B.5.2 Steering layer

We apply the steering to a specific layer inside the LLM, where the steering vector is computed using the output activations of the same layer. Fig. 28 shows that the steering is more effective in deeper layers. For instance, the number of original/target answers decrease/increase significantly while the accuracy on other answer types remains unchanged (layer 0 is considered the baseline).

B.5.3 Steering strength (α)

In this section, we study the effect of steering strength across different setups. In general, we find that increasing α leads to more steering effect. However, there is trade-off between the steering effect, targeted steering and the quality of the generated response.

Steering MLLMs answers. We steer the model to change an original answer towards a target one. Fig. 29 shows that increasing α pushes the model to generate the target answer more (as seen from the Answers count (target)). However, the steering becomes less targeted, as seen in the last column. For instance, the model starts generating the target answers even if the original answer is not included in the ground truth (gt/generated score).

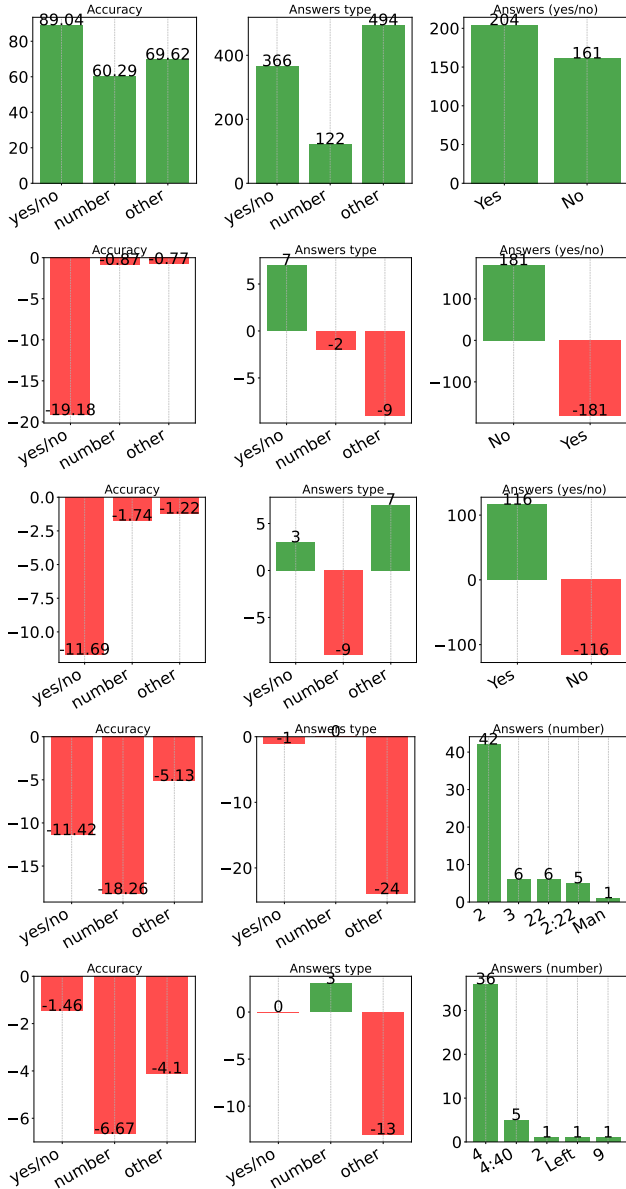


Figure 22. **Discovering meaningful steering directions.** Each line corresponds to a finegrained steering direction to steer the model answer to (from top to bottom): "No" (yes/no), "Yes" (yes/no), "2" (number) and "4" (number). First line corresponds to the original model without steering. Some steering directions are targeted (e.g., "No") as there is slight change in both the accuracy on other types (e.g., number, other) and the number of answers type.

Steering MLLMs answer types. Similarly, we vary α while changing the model answers to be from a particular type. Note that, here the steering should not be targeted as the goal is to change all answers (i.e., the steering vector is computed to steer the answers from random samples towards samples from a the target type). Fig. 30 shows that increasing α pushes the model to generate more answers from the target type. However, Fig. 31 shows that increasing the α significantly makes the model generate only few answers from the target type, which makes the generation

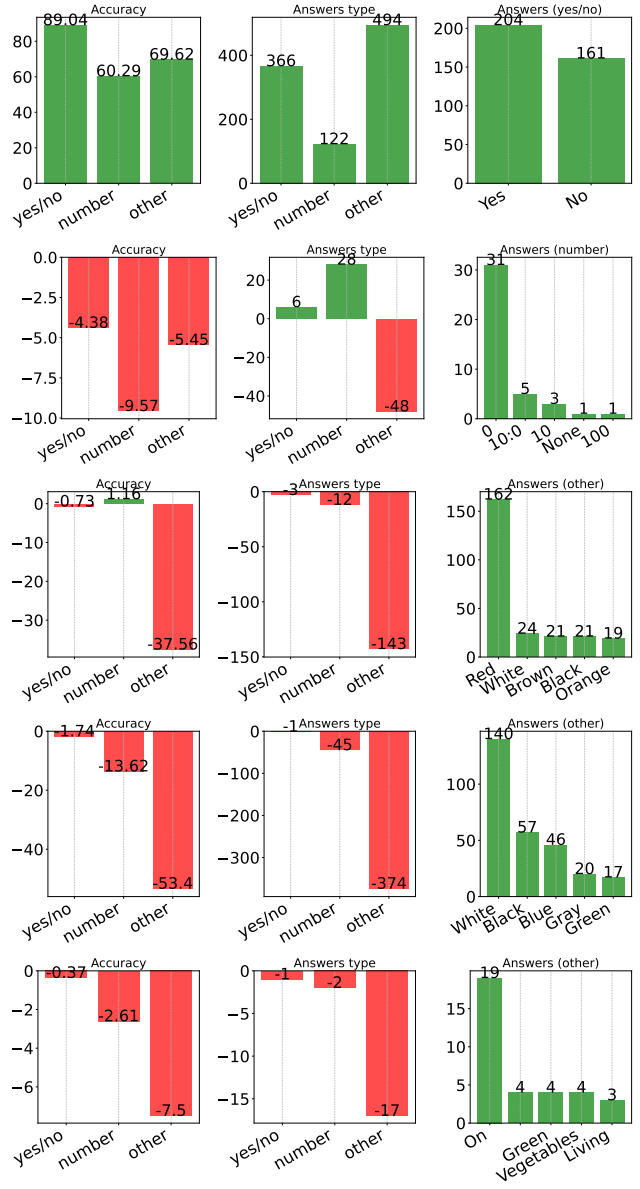


Figure 23. **Discovering meaningful steering directions.** Each line corresponds to a finegrained steering direction to steer the model answer to: "0" (number), "Red" (other), "White" (other) and "On" (other). First line corresponds to the original model without steering.

less diverse.

Steering MLLMs image caption styles. We also study the effect of steering strength on changing the captions styles. Fig. 32 shows, that increasing α leads the model to generate more captions from the target style. However, Fig. 33 shows that significantly increasing α degrades the quality of the generated captions as seen in the low CIDEr score. Note that, the CIDEr is expected to decrease as changing the caption style leads to deviation from the COCO annotated captions. However, the drastic decrease is due mainly to captions quality. We tried to inspect the output and found

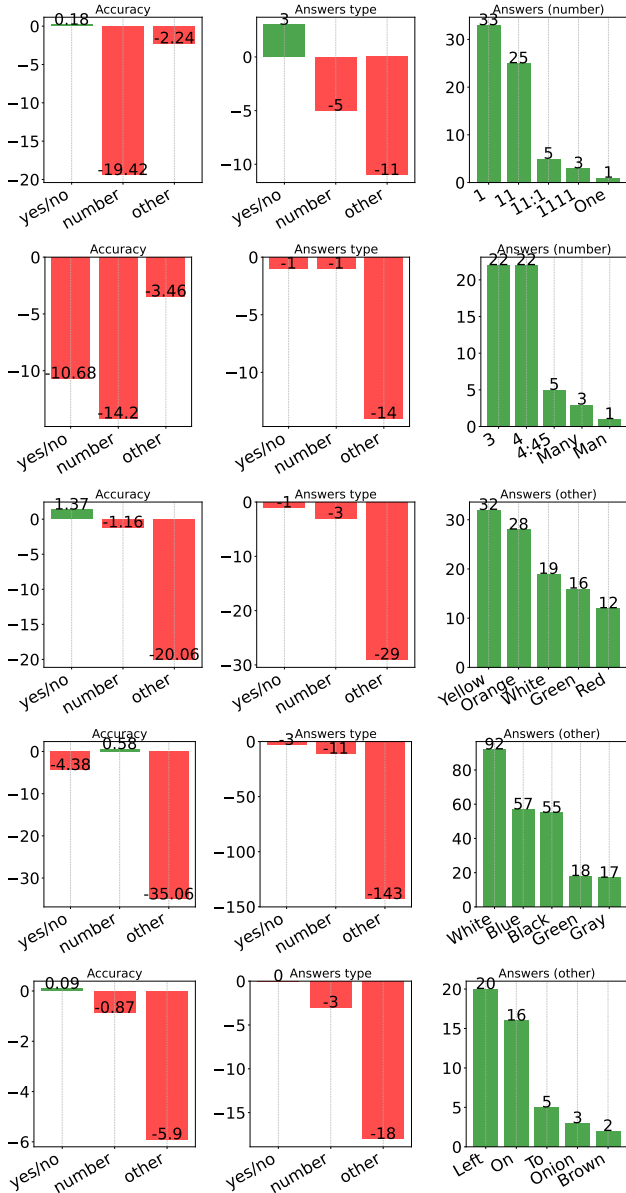


Figure 24. **Discovering meaningful steering directions towards multiple concepts.** Each line corresponds to a finegrained steering direction to steer the model answer to (from top to bottom): "1" and "11" (number), "3" and "4" (number), "Yellow" and "Orange" (other), "White" and "Blue" (other) and "Left" and "On" (other).

that sometimes the model only repeat 1 or 2 words related to the target type.

B.5.4 Which tokens to apply steering to?

In the main paper, we apply the steering vector to all tokens, including the image, instruction and generated ones. Here we study this design choice. Fig. 35 illustrates the results. We compare steering: all tokens including image, prompt and generated tokens ($I + T$), only text tokens (T , including the prompt and generated ones), only the generated tokens ($T(i = k)$) and last token in the prompt and

the generated tokens ($T(i \geq k - 1)$). Steering all tokens ($I + T$) has the most steering effect, followed by steering all text tokens (T). Steering only the generated tokens has little effect ($T(i = k)$), this can be significantly improved by steering the token just before ($T(i \geq k - 1)$).

B.6. Linear separability of concepts inside MLLMs.

In this section we investigate why a simple linear operation in the feature space, such as vector addition, is able to steer the model output. To this end, we visualize the PCA projections of the concepts features extracted from different layers inside MLLMs. Fig. 34 shows a clearer separation of concepts when moving to deeper layers, where different concepts can be almost separated linearly. This, to some extent, validates the linear representation hypothesis for MLLMs, previously studied for LLMs [32, 38]. In addition, this might explain why applying the steering to deeper layers is more effective than early ones.

B.7. Qualitative results

We provide additional qualitative results for steering MLLMs answers (Fig. 36), answer types (Fig. 37) and caption styles (Fig. 38)

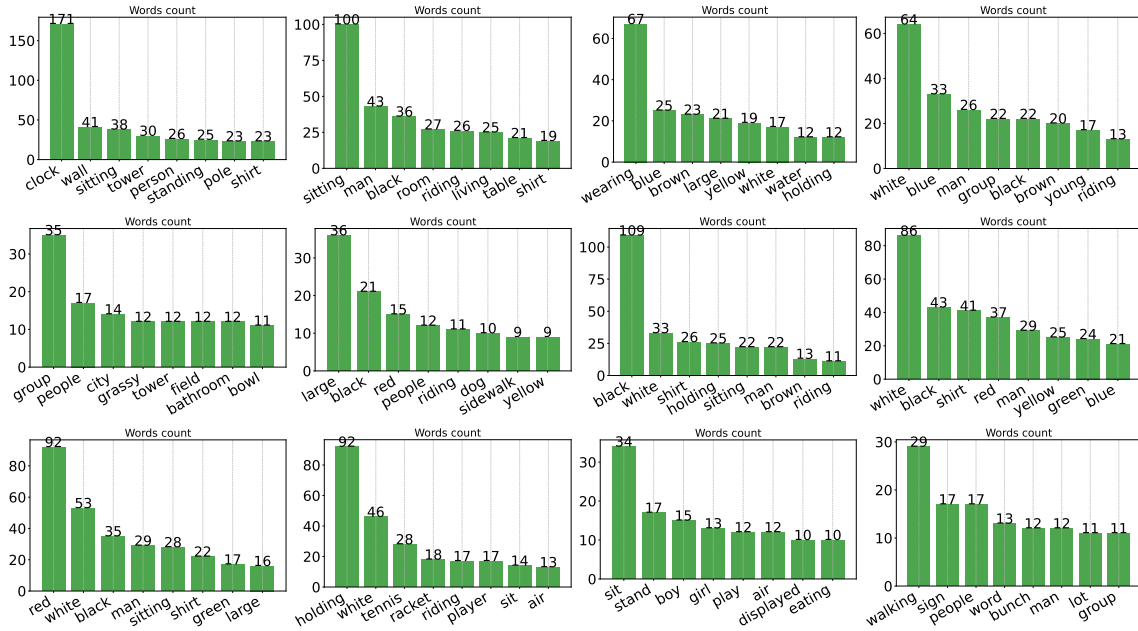


Figure 25. **Discovering meaningful steering directions with image captioning.** We report the relative increase in number of words counts. Each figure corresponds to different fine-grained steering direction.

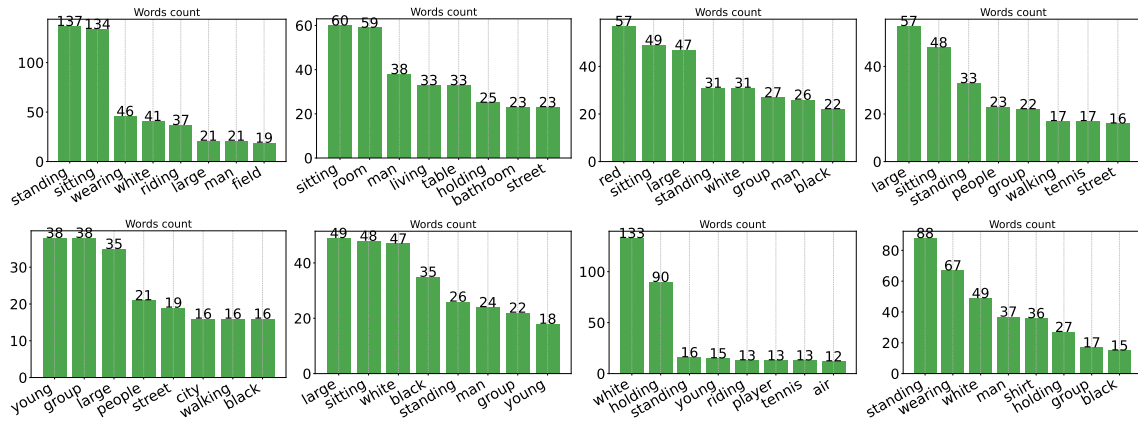


Figure 26. **Discovering meaningful steering directions with image captioning towards multiple concepts.** We report the relative increase in number of words count. Each figure corresponds to different fine-grained steering direction towards multiple concepts.

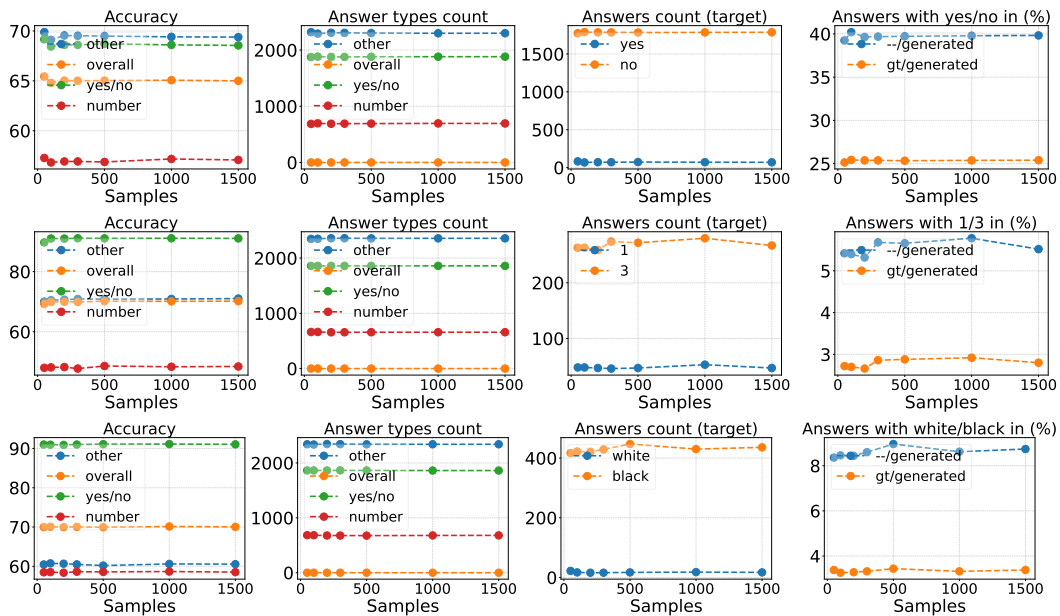


Figure 27. **Ablation study: number of samples to compute steering vector.** From top to bottom: steering answers from "Yes" (yes/no), "1" (number), "White" (other) to "No", "3", "Black" respectively. We report different metrics as follows (from left to right): VQA accuracy per answer type, number of answers belonging to each type, number of occurrence of the original and target answers (*e.g.*, yes and no), number of answers that contain the target answers (-/generated) and in addition the original answer in the ground truth (gt/generated). Computing the steering vector is robust to varying the number of samples.

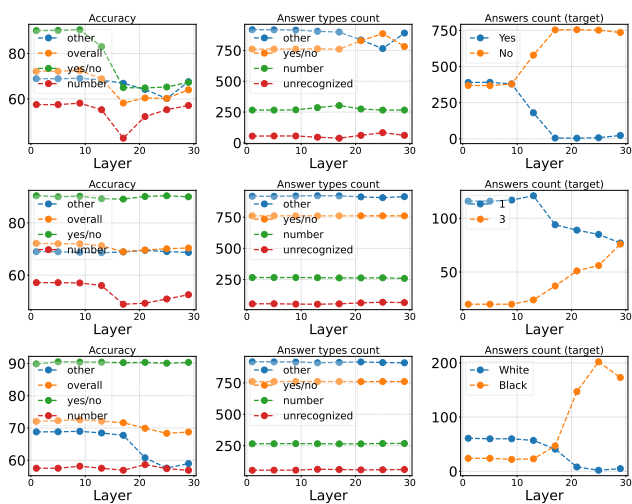


Figure 28. **Ablation study: steering MLLMs across layers.** From top to bottom, steering answers from: "Yes" (yes/no), "1" (number), "White" (other) to "No", "3", "Black" respectively. Steering is more effective in deeper layers as the number of original/target answer counts decrease/increase significantly. In last layers, the accuracy on other answers type changes slightly, and the number of answers types count remains almost constant.

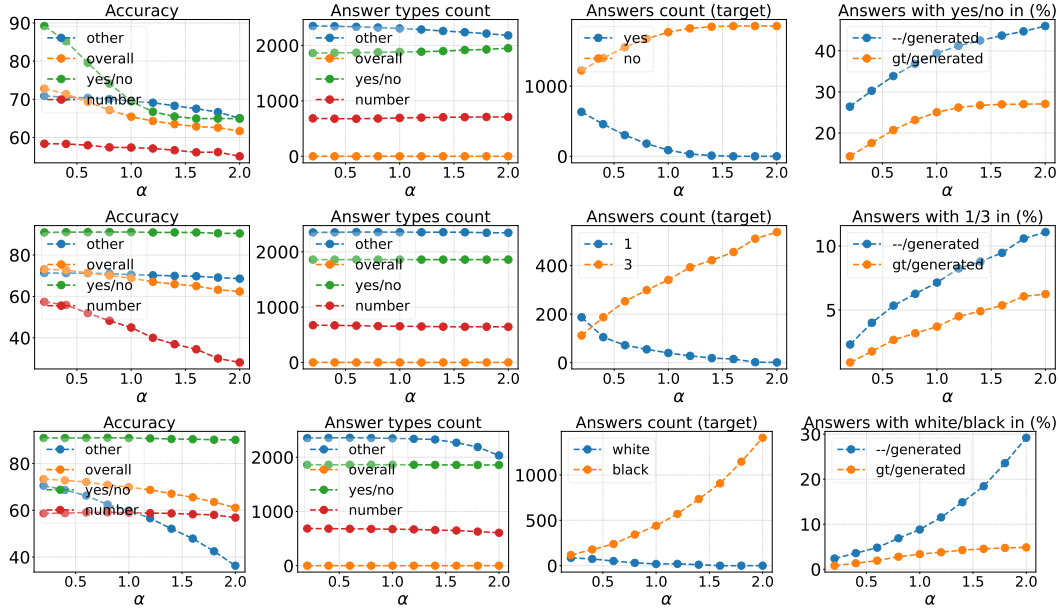


Figure 29. **Ablation study: steering strength (α)**. From top to bottom: steering answers from "Yes" (yes/no), "1" (number), "White" (other) to "No", "3", "Black" respectively. We report different metrics as follows (from left to right): VQA accuracy per answer type, number of answers belonging to each type, number of occurrence of the original and target answers (*e.g.*, yes and no), number of answers that contain the target answers (*-/generated*) and in addition the original answer in the ground truth (*gt/generated*). Increasing α pushes the model to generate more the target answer. However, the steering becomes less targeted, as seen in the last column.

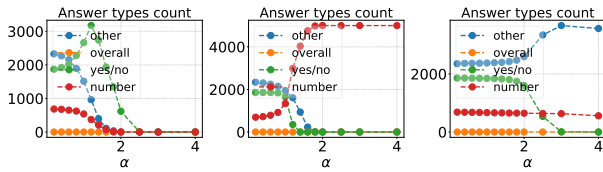


Figure 30. **Ablation study: steering strength (α) and changing answer types**. From left to right: steering answers type towards: yes/no, number and other. We report the number of answers in each answer type. Increasing α pushes the model to generate more answers from the target type.

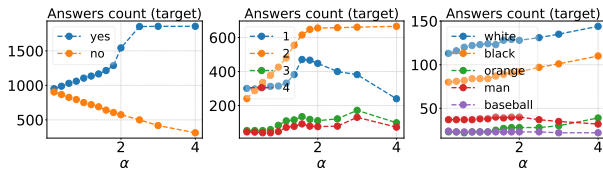


Figure 31. **Ablation study: steering strength (α) and changing answer types**. From left to right: steering answers type towards: yes/no, number and other. We report the number of occurrences of some answers in each type. Increasing α pushes the model to generate few answers significantly more than others.

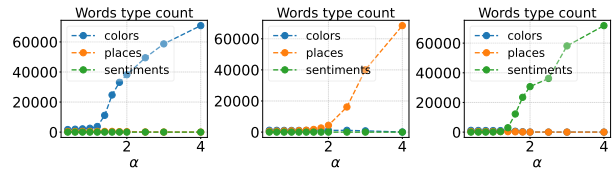


Figure 32. **Ablation study: steering strength (α) and changing caption styles**. From left to right: steering captions style to include more: colors, places and sentiments. We report the number words belonging to each type. Increasing α pushes the model to generate words related to the target style.

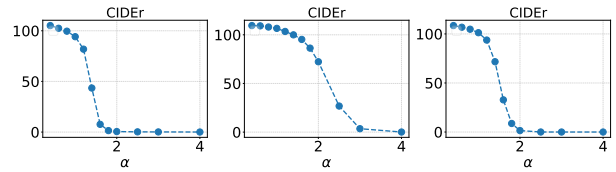


Figure 33. **Ablation study: steering strength (α) and changing caption styles**. From left to right: steering captions style to include more: colors, places and sentiments. We report the CIDEr score. Despite having more captions from the target style, significantly increasing α leads to significant degradation in captioning quality. Note that the CIDEr is expected to decrease as changing the style deviates the captions more from the ground truth. However, we see huge drop when α goes beyond 1.

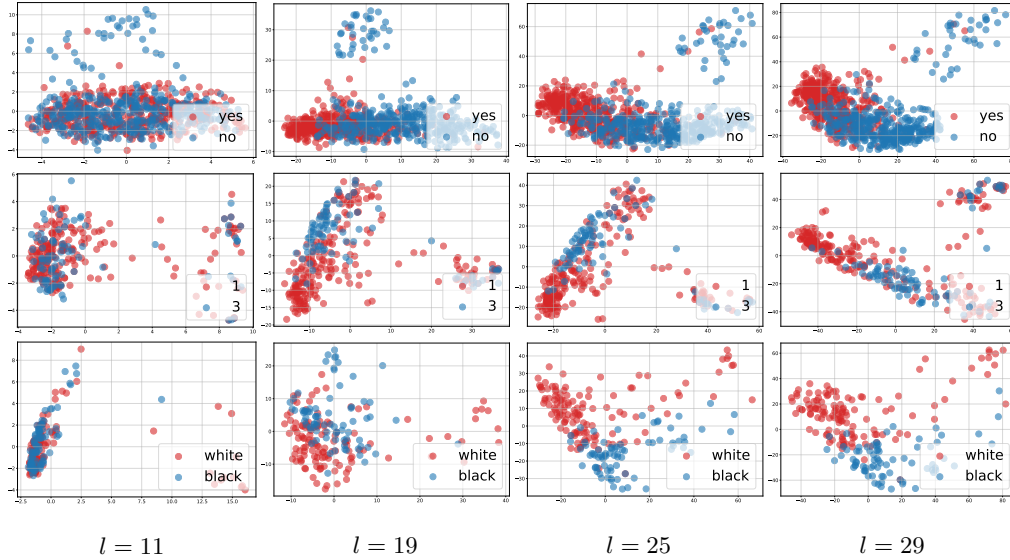


Figure 34. **Linear separability of concepts features in MLLMs.** We visualize the features related to the concepts "yes"/"no", "1"/"3" and "white"/"black" after PCA projections across MLLMs layers.

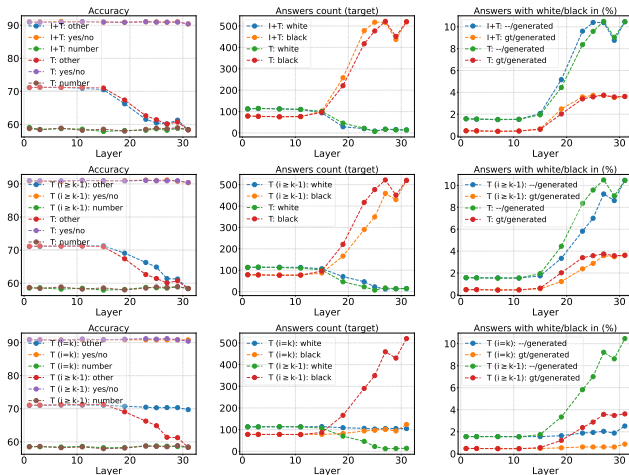


Figure 35. **Ablation study: which tokens to apply steering to.** We compare steering: all tokens including image, prompt and generated tokens ($I + T$), only text tokens (T , including the prompt and generated ones), only the generated tokens ($T(i = k)$) and last token in the prompt and the generated tokens ($T(i \geq k - 1)$). Steering all tokens ($I + T$) has the most steering effect, followed by steering all text tokens (T). Steering only the generated tokens has little effect ($T(i = k)$), this can be fixed by steering the token just before ($T(i \geq k - 1)$)



What color is the airplane?

↓



What color is the sign written in?

↓



What color is the skier's helmet?

↓



How many towels?

↓



How many pictures are on the wall?

↓



How long until the clock says midnight?

↓



Does the boat resemble a car?

↓



Is the giraffe taller than the grass?

↓



Is this vegetable high in beta carotene?

↓

Figure 36. **Steering MLLMs answers.** Each line corresponds to different steering vector that change a specific original answer to a **target** one. From top to bottom: "white" to "black", "1" to "3" and "yes" to "no".

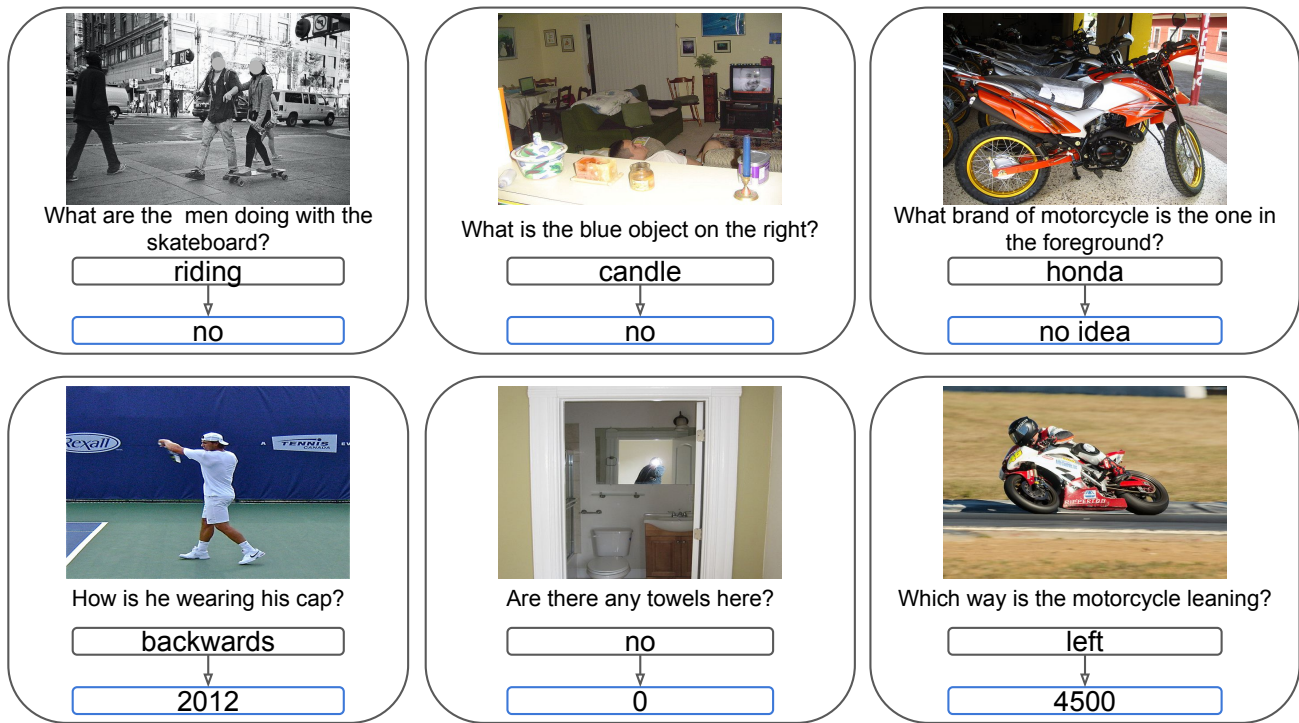


Figure 37. **Steering MLLMs answers type.** Each line corresponds to different steering vector that change answers type to a [target](#) one. Steering vectors correspond to changing the answers type to yes/no (top) and numbers (bottom).

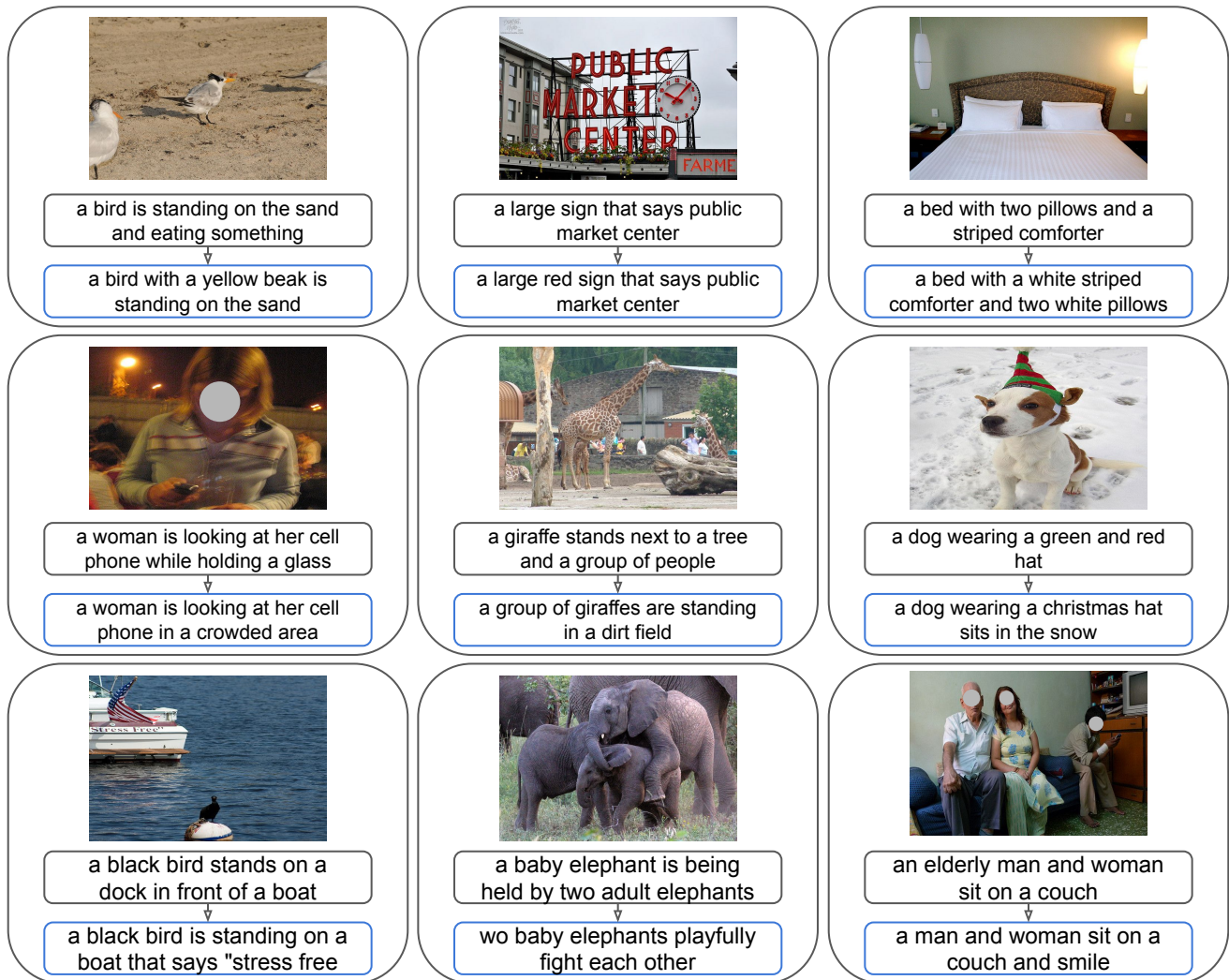


Figure 38. **Steering MLLMs captions type.** Each line corresponds to different steering vector that change captions style to a [target](#) one. Steering vectors correspond to changing the captions style so that they contain more: colors (top), places (middle) and sentiments (bottom).